Therapeutic inhibition of acid sensing ion channel 1a recovers heart function after ischemia-reperfusion injury

Meredith A. Redd[1,2†], Sarah E. Scheuer[3,4,5†], Natalie J. Saez[1], Yusuke Yoshikawa[6], Han S. Chiu[1], Ling Gao[3], Mark Hicks[3,5,7], Jeanette E. Villanueva[3,5], Gabriel Cuellar-Partida[8], Jason N. Peart[9], Louise E. See Hoe[2,10], Xiaoli Chen[1], Yuliangzi Sun[1], Jacky Y. Suen[2,10], Robert J. Hatch[11], Ben Rollo[11], Mubarak A.H. Alzubaidi[1], Snezana Maljevic[11], Gregory A. Quaife-Ryan[12], James E. Hudson[12], Enzo R. Porrello[13,14], Melanie Y. White[15], Stuart J. Cordwell[15], John F. Fraser[2,10], Steven Petrou[11], Melissa E. Reichelt[6], Walter G. Thomas[6], Glenn F. King[1]*, Peter S. Macdonald[3,4,5]* & Nathan J. Palpant[1]*

[1]Institute for Molecular Bioscience, The University of Queensland, St. Lucia, Australia.
[2]Critical Care Research Group, The Prince Charles Hospital and The University of Queensland, Brisbane, Australia.
[3]Victor Chang Cardiac Research Institute, Sydney, Australia.
[4]Cardiopulmonary Transplant Unit, St. Vincent's Hospital, Sydney, Australia.
[5]Faculty of Medicine, University of New South Wales, Sydney, Australia.
[6]School of Biomedical Sciences, The University of Queensland, St. Lucia, Australia
[7]Department of Pharmacology, St. Vincent's Hospital, Sydney, Australia.
[8]The University of Queensland Diamantina Institute, Faculty of Medicine and Translational Research Institute, Woolloongabba, Australia.
[9]School of Medical Science, Griffith University, Southport, Australia.
[10]Faculty of Medicine, The University of Queensland, Brisbane, Australia.
[11]Florey Institute of Neuroscience and Mental Health, The University of Melbourne, Melbourne, Australia.
[12]QIMR Berghofer Medical Research Institute, Brisbane, Australia.
[13]Murdoch Children's Research Institute, The Royal Children's Hospital, Melbourne, Australia.
[14]Department of Physiology, School of Biomedical Sciences, The University of Melbourne, Parkville, Australia.
[15]School of Medical Sciences, The University of Sydney, Sydney, Australia
†These authors contributed equally.
*Corresponding authors.

Addresses for correspondence:
Dr. Nathan J. Palpant
Institute for Molecular Bioscience
306 Carmody Road, Building 80 (Level 4 North)
St. Lucia, Queensland, Australia, 4072
T: +61 7 3346 2054; E: n.palpant@imb.uq.edu

Professor Glenn F. King
Institute for Molecular Bioscience
306 Carmody Road, Building 80 (Level 2 North)
St. Lucia, Queensland, Australia, 4072
T: +61 7 3346 2025; E: glenn.king@imb.uq.edu.au

Professor Peter Macdonald
Cardiopulmonary Transplant Unit, St. Vincent's Hospital
Darlinghurst, New South Wales, Australia
T: +61 2 8382 2641; E: peter.macdonald@svha.org.au

Abstract

Ischemia-reperfusion injury (IRI) is one of the major risk factors implicated in morbidity and mortality associated with cardiovascular disease. Here we show that the proton-gated acid-sensing ion channel 1a (ASIC1a) plays a key role during cardiac ischemia and demonstrate that ASIC1a is a promising therapeutic target to improve the tolerance of cardiac tissue to IRI. Genetic ablation of ASIC1a leads to improved functional recovery following global myocardial IRI in *ex vivo* mouse hearts, and this effect can be recapitulated by therapeutic blockade of ASIC1a using specific and potent pharmacological inhibitors. We used two models of *ex vivo* donor heart procurement and storage, an *in vivo* model of myocardial infarction, and *in vitro* studies using human iPSC-derived cardiomyocytes to show that ASIC1a inhibition improves post-IRI cardiac viability. Use of ASIC1a inhibitors as pre- or post-conditioning agents provided equivalent cardioprotection to benchmark drugs, including the sodium-hydrogen exchange inhibitor zoniporide. At the cellular and whole organ level, we show that acute exposure to ASIC1a inhibitors has no impact on cardiac ion channels regulating baseline electromechanical coupling and physiological performance. Collectively, our data provide compelling evidence for a novel pharmacological strategy involving ASIC1a blockade as a cardioprotective therapy to improve the viability of donor hearts exposed to myocardial ischemia.

Introduction

Conditions caused by obstruction of blood flow to the heart are the most common emergency manifestation of cardiovascular disease(*7*). Although acute reperfusion therapies have improved patient outcomes, mortality remains high(*8*) and MI is one of the largest attributable risks for heart failure (HF)(*9*). Globally, 1 in 5 people develop HF, with annual healthcare costs of $108B(*10, 11*). Heart transplantation remains the most effective treatment option for HF(*12, 13*), but 75% of potential donor hearts are discarded, many due to sensitivity of the donor heart to ischemic injury(*14*). Myocardial sensitivity to ischemia-reperfusion injury (IRI) therefore remains a primary point of vulnerability underlying cardiovascular disease, which is the leading cause of morbidity and mortality worldwide(*15*). Despite decades of preclinical therapeutic development, there are no drugs that block the acute injury response to cardiac ischemia(*16*).

Myocardial IRI is a complex pathophysiological process that underlies the cardiac injury sustained during cardiac surgery, heart transplant, MI, and cardiac arrest. During myocardial ischemia, reduced oxygen availability causes a shift from fatty acid metabolism to anaerobic glycolysis(*17, 18*). The resulting lactic acidosis causes a significant drop in both extracellular and intracellular pH, reaching as low as 6.0–6.5(*19-23*). In patients suffering from acute MI, the severity of metabolic acidosis strongly correlates with patient mortality, with serum pH < 7.35 associated with > 60% mortality(*24*).

At the cellular level, acidosis results in the activation of several transmembrane ion channels and receptors, including the sodium-hydrogen exchanger (NHE), glutamate-gated NMDA receptors, and the TRP family of ion channels, each of which are thought to contribute to calcium overload, metabolic dysfunction, and eventually cell death(*25-27*). In line with this, the Expedition Trial showed that the NHE inhibitor, cariporide, provided significant protection against peri-operative MI in patients undergoing high-risk coronary artery bypass surgery(*28*). While this trial failed due to cerebrovascular complications, it demonstrated that pharmacological conditioning has the capacity to reduce the injury response to myocardial IRI.

Acid sensing ion channels (ASICs) are voltage-independent proton-gated cation channels of the degenerin/epithelial sodium channel superfamily(*29*). There are six ASIC isoforms derived from four genes (*ACCN1–4*), which assemble into homotrimeric or heterotrimeric channels. The pH sensitivity and kinetics of ASICs are determined by their subunit composition(*30, 31*). ASICs are involved in extracellular acidification-induced calcium overload in neurons and cardiomyocytes(*32-34*). ASIC1a, a splice variant of the *ACCN1* gene, is the most pH-sensitive ASIC channel. Activation begins at pH ≤ 7, with half-maximal activation at pH 6.6(*35, 36*), and ASIC1a currents are potentiated by numerous metabolic events that occur during ischemia, including membrane stretch and increased levels of extracellular lactate, pyruvate, and arachidonic acid(*37, 38*). ASIC1a plays a critical role in mediating ischemia-induced neuronal death, and inhibition of ASIC1a through genetic ablation or pharmacological blockade is neuroprotective in rodent models of ischemic stroke(*2, 39, 40*).

In this study, we used genetic and pharmacological approaches to demonstrate that ASIC1a is a critical mediator of the injury response to myocardial IRI. We show that venom-derived inhibitors of ASIC1a provide robust cardioprotection across multiple species and model systems from the cellular to whole-organ level, including *ex vivo* models of IRI and donor heart preservation, and an *in vivo* model of MI. Taken together, our data provide compelling support for ASIC1a as a target for cardioprotective drugs, with potential application in the treatment of ischemic injuries of the heart.

Results

Genetic ablation of ASIC1a improves functional recovery following cardiac IRI

We assessed ASIC isoform expression in the adult mouse heart using transcriptomic data of sorted cardiac cell populations(*6*). *ASIC1* expression was highest in cardiomyocytes, while endothelial cells and fibroblasts expressed both *ASIC1* and *ASIC3*. In all three cell types,

Table 1. Baseline functional parameters of isolated hearts from wild-type and ASIC1a KO mice

Genotype	Heart Rate (bpm)	LVDP (mmHg)	EDP (mmHg)	+dP/dt (mmHg/s)	-dP/dt (mmHg/s)	CF (mL/min/g)
Wildtype (ASIC1a$^{+/+}$)	353 ± 23	105 ± 4	6.8 ± 0.7	3777 ± 139	–2592 ± 144	35 ± 5
KO (ASIC1a$^{-/-}$)	339 ± 17	101 ± 4	5.1 ± 0.7	3647 ± 236	–2702 ± 148	26 ± 3
p-value	*0.67*	*0.54*	*0.13*	*0.66*	*0.64*	*0.25*

All pre-ischemia functional parameters were measured in Langendorff perfused hearts after more than 30 min of stabilization, except for heart rate, which was measured after 15 min of stabilization, prior to ventricular pacing. All values are expressed as mean ± SEM.

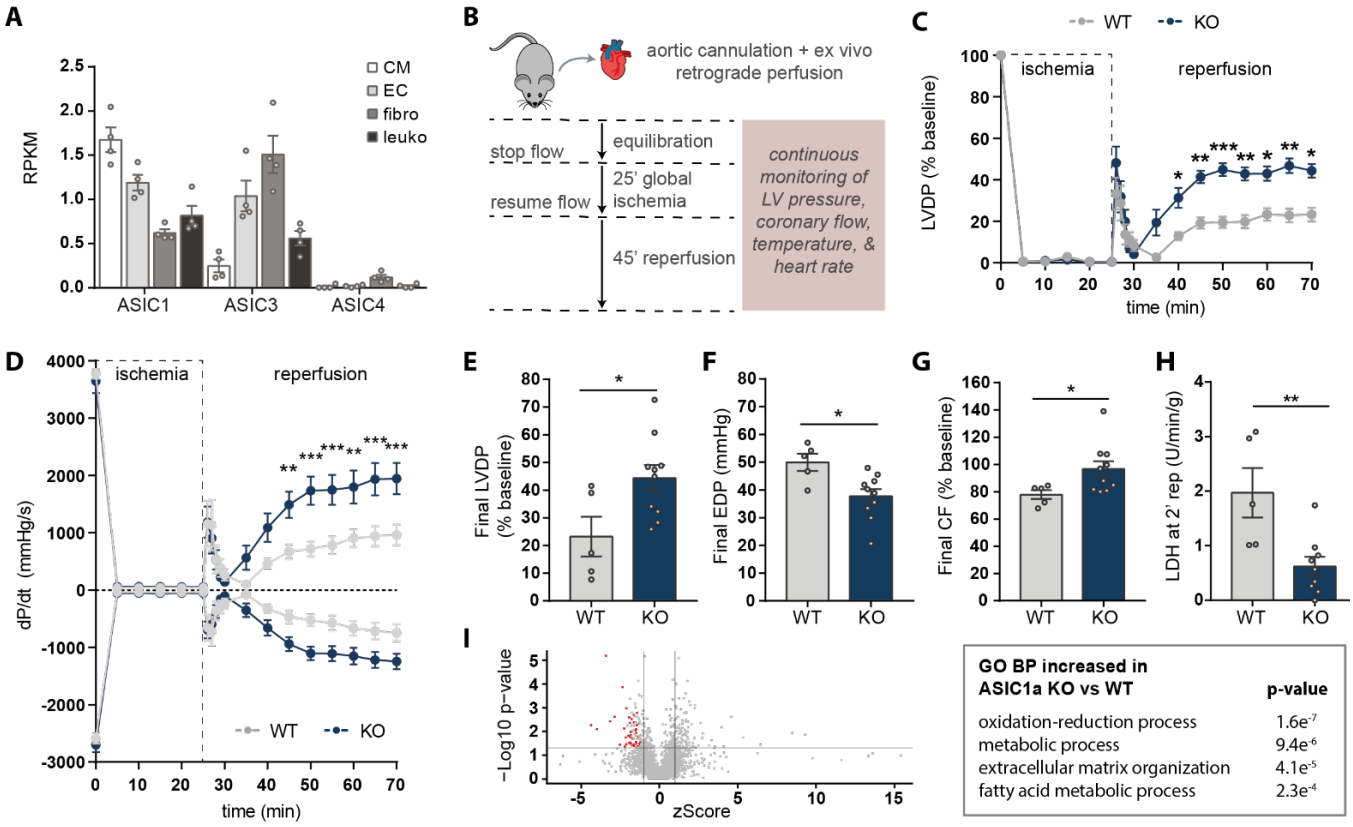

Figure 1. Genetic knockout of ASIC1a protects mouse hearts from *ex vivo* IRI. (**A**) mRNA expression (reads per kilobase million, RPKM) analysis of sorted cardiac cell populations from P56 adult mouse hearts (data extracted from Ref. (*6*)). ASIC2 was not detected. (**B-F**) Langendorff-perfused hearts from ASIC1a KO (ASIC1a$^{-/-}$, n = 10) and WT (ASIC1a$^{+/+}$, n = 5) mice were subjected to 25 min of global ischemia followed by 45 min of reperfusion. (**C**) LVDP, expressed as % of pre-ischemia baseline, over time. (**D**) Positive and negative rate of change in pressure over time in ASIC1a KO vs WT hearts. **(E-F)** Functional parameters after 45 min of reperfusion including **(E)** LVDP, percent baseline (p = 0.025) and (**F**) EDP, p = 0.013. (**G**) CF, percent baseline (p = 0.049). (**H**) Cell death after 2 min of reperfusion (units/mL of LDH normalized to reperfusion flow rate and heart weight, U/min/g, p = 0.006). For LVDP and CF, baseline values were obtained immediately prior to ischemia. **(I)** Quantitative proteomic analysis showing volcano plot and all biological processes significantly increased in ASIC1a KO hearts compared to WT. All data are expressed as mean ± SEM. Statistical significance was determined using two-way ANOVA (panels c and d) or two-tailed unpaired Student's *t*-test (panels e-h) (*p < 0.05; **p < 0.01; ***p < 0.001).

ASIC4 and *ASIC2* had low and undetectable expression, respectively (**Figure 1A**). *ASIC1* encodes two isoforms from the same genetic locus, ASIC1a and ASIC1b, that are genetically conserved in bilaterians. As opposed to ASIC1b, which is primarily involved in nociception(*41*), we focused on ASIC1a due to its known role in mediating ischemic injuries of the brain(*31*).

To determine whether ASIC1a plays a functional role during cardiac ischemia, we assessed IRI tolerance of Langendorff-perfused isolated hearts from ASIC1a-specific knockout (KO) mice. To generate the ASIC1a KO mouse strain, we used CRISPR editing to target the *ACCN1* locus. Specificity of the knockout was confirmed using qRT-PCR, which showed that only *ASIC1a*, but not *ASIC1b* mRNA was reduced in brain tissue from KO mice (**Supplemental Figure 1A-B**). Baseline function and heart rate in ASIC1a KO (ASIC1a$^{-/-}$) isolated hearts were comparable to those measured in wild-type (WT) control hearts (ASIC1a$^{+/+}$) (**Table 1**). To assess tolerance to IRI, hearts were subjected to 25 min of global normothermic zero-flow ischemia, followed by 45 min of aerobic reperfusion **(Figure 1B)**. WT and ASIC1a KO hearts showed similar initial responses to ischemia with comparable levels of ventricular contracture (**Supplemental Figure 1C**). During reperfusion, both groups demonstrated gradual recovery of contractile function over time, with markedly improved contractile recovery in ASIC1a KO hearts as measured by LVDP and dP/dt (**Figure 1C-D**). By the end of the reperfusion period, ASIC1a KO hearts had significantly higher left ventricular developed pressure (LVDP) (44 ± 5% of baseline) and lower end diastolic pressure (EDP) (38 ± 3 mmHg) compared to WT hearts (LVDP: 23 ± 7% of baseline; EDP: 50 ± 3 mmHg); **Figure 1E-F**). ASIC1a KO hearts also had improved recovery of coronary flow (CF) by the end of reperfusion (KO: 97 ± 6%; WT: 78 ± 3%, percent baseline) (**Figure 1G** and **Supplemental Figure 1D-E**). To assess cell death, lactate dehydrogenase (LDH) efflux

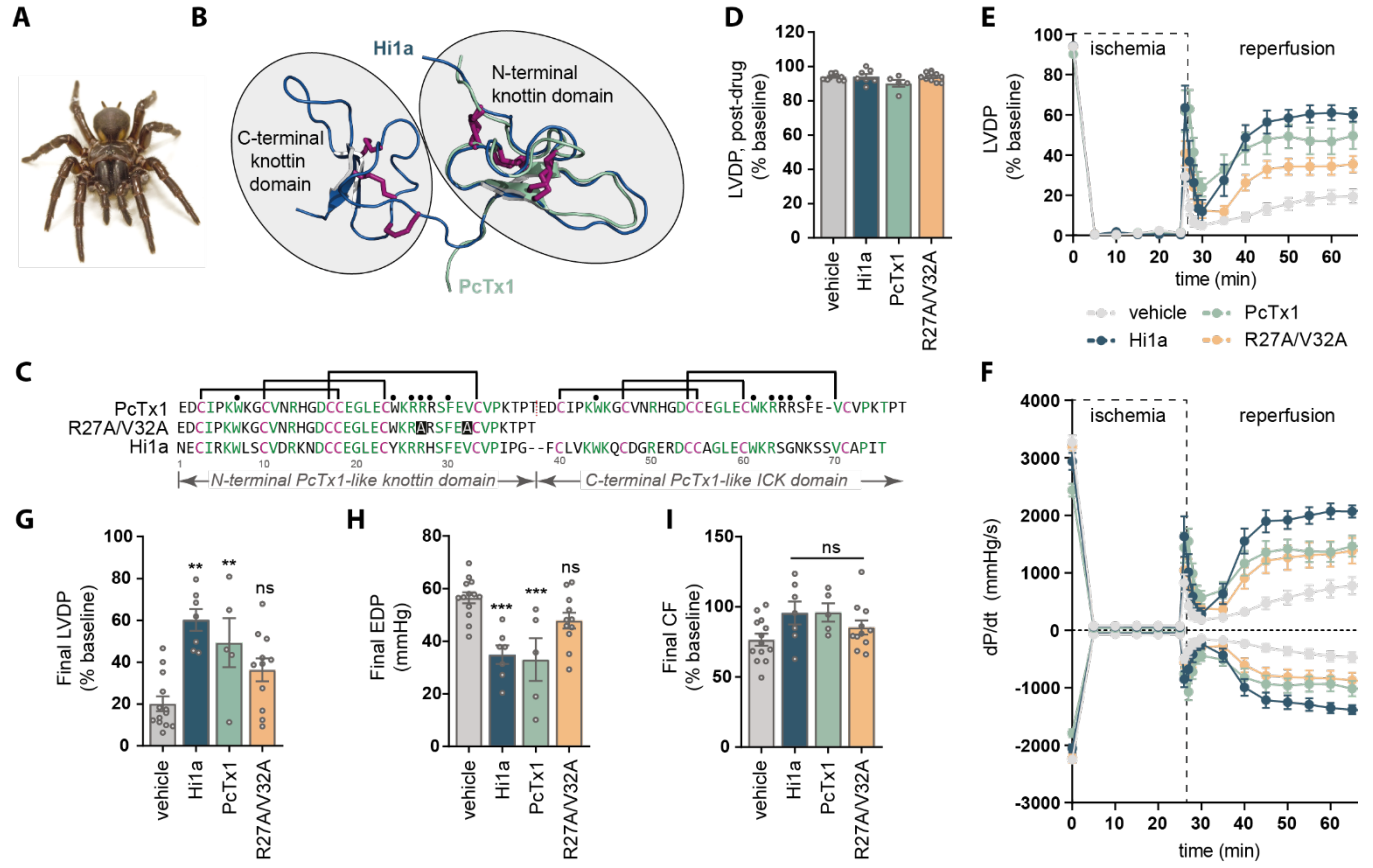

Figure 2. ASIC1a inhibitors protect isolated mouse hearts from IRI. (**A**) Australian funnel-web spider, *Hadronyche infensa*, from which the ASIC1a inhibitor Hi1a was isolated. (**B**) Schematic of the 3D structure of Hi1a (PDB 2N8F (*2*)) highlighting the two knottin domains. The 3D structure of PcTx1 (green; PDB 2KNI (*3*)) is overlaid on the N-terminal knottin domain of Hi1a (blue). The disulfide bonds in each structure are shown as maroon tubes. (**C**) Sequence alignment of Hi1a, PcTx1, and the PcTx1-R27A/V32A analogue. Conserved residues are shown in green, except cysteine residues which are highlighted in maroon. Black circles indicate pharmacophore residues of PcTx1. (**D-H**) Langendorff-perfused hearts from adult (12–14 weeks old) male C57BL/6 mice were subjected to 25 min of global ischemia followed by 45 min of reperfusion. Control hearts (no treatment, $n = 21$) were compared to hearts treated with 10 nM Hi1a ($n = 7$), 10 nM PcTx1 ($n = 5$), 10 nM PcTx1-R27A/V32A, $n = 11$), or 0.1% BSA in water (vehicle control, $n = 13$). For treated hearts, vehicle or peptide solution was infused for 10 min prior to ischemia and during the first 15 min of reperfusion. (**D**) Pre-ischemia LVDP, expressed as % baseline, after exposure to vehicle or peptide for 10 min. (**E**) LVDP over time. **(F)** Positive and negative rate of change in pressure over time in hearts treated with Hi1a or PcTx1 variants vs vehicle. (**G-I**) Functional parameters measured or calculated after 45 min of reperfusion including (**G**) LVDP (**H**) EDP and (**I**) CF. For LVDP and CF, baseline values were obtained prior to peptide/vehicle infusion, or 10 min prior to onset of ischemia (no-infusion controls). All data are expressed as mean ± SEM. Statistical significance was determined using one-way ANOVA with multiple comparisons (**p < 0.01, ***p < 0.001).

was measured in perfusate samples collected during reperfusion. LDH efflux from ASIC1a KO hearts was significantly lower compared to WT hearts after 2 min of reperfusion (**Figure 1H**), with a similar trend at the end of reperfusion (**Supplemental Figure 1F**). Our data indicate that ASIC1a does not play a role in maintaining functional homeostasis, but it is a critical mediator of the organ response to myocardial IRI.

To determine underlying molecular differences between ASIC1a and WT hearts, we performed unsupervised quantitative liquid chromatography mass spectrometry (LC MS/MS) on hearts collected at the end of reperfusion (**Supplemental Table 2**). Among proteins with significantly different abundance, gene ontology analysis revealed no significant differences in down-regulated biological processes in ASIC1a KO vs WT hearts. However, ASIC1a KO hearts showed significant increases in proteins related to oxidation-reduction, fatty acid metabolism, and extracellular matrix organisation **(Figure 1I** and **Supplemental Figure 1G-H)**. These data suggest that improved survival and functional performance of ASIC1a hearts is at least in part mediated through increased abundance of molecules maintaining metabolic and structural homeostasis under conditions of severe acute myocardial ischemia.

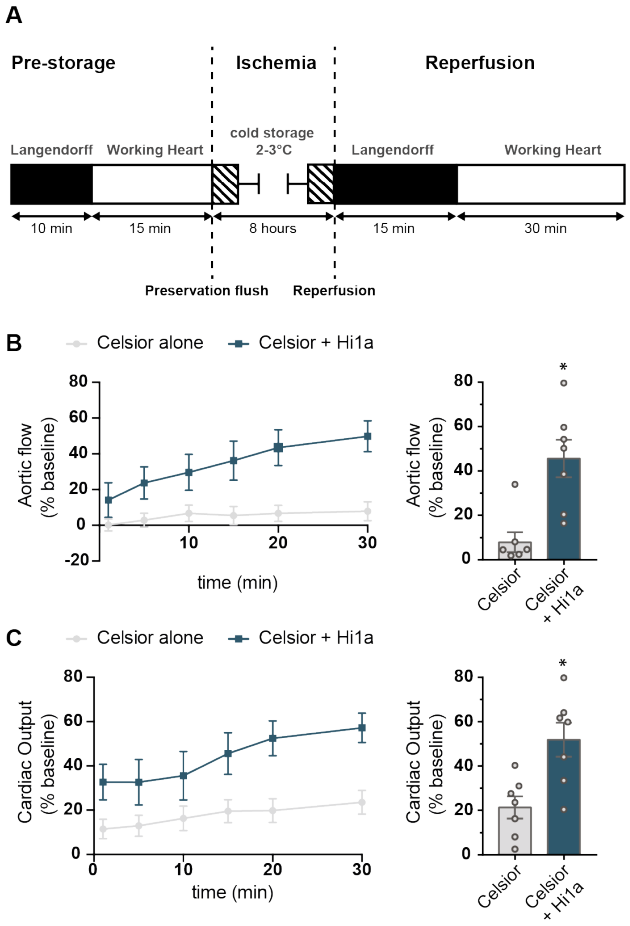

Figure 3. Hi1a protects isolated rat hearts during long-term hypothermic storage. (**A**) Experimental schematic of 8 h cold storage protocol. (**B-C**) Functional parameters assessed throughout 30 min working mode (post-storage reperfusion) and normalized to pre-storage function. (**B**) Aortic flow (% baseline) over time (left) and after 30 min (right). (**C**) Cardiac output (% baseline) over time (left) and after 30 min (right). All data are expressed as mean ± SEM (n = 7 per group). Statistical significance was determined using two-tailed unpaired Student's t-test (*p < 0.05).

ASIC1a inhibitors protect mouse hearts against IRI

We sought to determine whether pharmacological inhibition of ASIC1a is cardioprotective during an acute cardiac ischemic insult. Despite significant investment and preclinical testing, drug development pipelines have failed to identify effective small molecule inhibitors of ASIC1a with therapeutically useful specificity, potency, and functional efficacy(*42-44*). We therefore took advantage of two venom-derived peptides that are both potent and selective inhibitors of ASIC1a, with no activity on other ASIC isoforms(*2, 39*). Hi1a is a 76-residue double-knot peptide isolated from the venom of an Australian funnel-web spider (**Figure 2A**); it is the most potent and selective inhibitor of ASIC1a identified to date, with an IC_{50} on rat and human ASIC1a of ~500 pM (*2*). PcTx1, a single-knot peptide from the venom of a tarantula, is also a potent and selective inhibitor of ASIC1a (IC_{50} ~1 nM) (*39*). Although the two peptides are closely related (Hi1a is comprised of two PcTx1-like domains joined by a short linker; **Figure 2B-C**), they have distinct inhibitory modes of action. Hi1a inhibits ASIC1a activation whereas PcTx1 promotes and stabilizes a desensitized state of the channel(*2*). We also utilized an analogue of PcTx1 that contains mutations of two pharmacophore residues (R27A/V32A), which dramatically reduces its inhibitory effect on ASIC1a(*39*).

To examine if these ASIC1a inhibitors are cardioprotective, we assessed tolerance to IRI in Langendorff-perfused isolated mouse hearts with and without peptide treatment. Consistent with genetic ablation of ASIC1a, Hi1a, PcTx1, and PcTx1-R27A/V32A had no effect on baseline contractile function during the first 10 min of peptide infusion prior to ischemia (**Figure 2D**). Contractile recovery after IRI measured by LVDP and dP/dt was greater in hearts exposed to Hi1a or PcTx1 (10 nM) compared to control hearts (**Figure 2E-F**). At the end of reperfusion, Hi1a- and PcTx1-treated hearts, but not hearts treated with the PcTx1-R27A/V32A analogue, had markedly improved recovery of LVDP (Hi1a: 60 ± 4%, PcTx1: 49 ± 12%, PcTx1-R27A/V32A: 36 ± 6%) compared to vehicle controls (20 ± 4%) (**Figure 2G**). Similarly, treatment with Hi1a and PcTx1, but not PcTx1-R27A/V32A, led to reduced EDP after 45 min reperfusion (Hi1a: 35 ± 4 mmHg; PcTx1: 33 ± 8 mmHg; PcTx1-R27A/V32A: 48 ± 3 mmHg) compared to vehicle controls (57 ± 2 mmHg) (**Figure 2H**). No differences in final CF were observed between groups (**Figure 2I**), although hearts treated with PcTx1, but not Hi1a, displayed significant reactive hyperaemia during early reperfusion, as evidenced by increased CF during the first 5 min of reperfusion (**Supplemental Figure 2A**,**B**). To demonstrate specificity of Hi1a, we show that exposure of hearts to Hi1a in an ASIC1a KO background shows no additive effect in functional recovery after global IRI **(Supplemental Figure 2C-F)**. Taken together, our data show that ASIC1a inhibitors protect the heart from myocardial IRI and recapitulate the functional benefits of genetic ablation of the channel.

Preconditioning with Hi1a improves functional recovery of isolated rodent hearts after prolonged hypothermic ischemia

In order to evaluate the cardioprotective effect of ASIC1a inhibition in a model of donor heart preservation, we supplemented standard clinical heart preservation solution (Celsior(*45*)) with Hi1a during 8 h cold storage of isolated rat hearts. The hearts were stabilised for 10 min by retrograde (Langendorff) perfusion and then switched to working-mode in order to assess cardiac function in the presence of physiological afterload. Following assessment of baseline hemodynamic parameters, hearts were arrested by infusion of cold (2–3°C) Celsior solution with and without 10 nM Hi1a into the coronary circulation. After cardioplegic arrest, hearts were stored under hypothermic

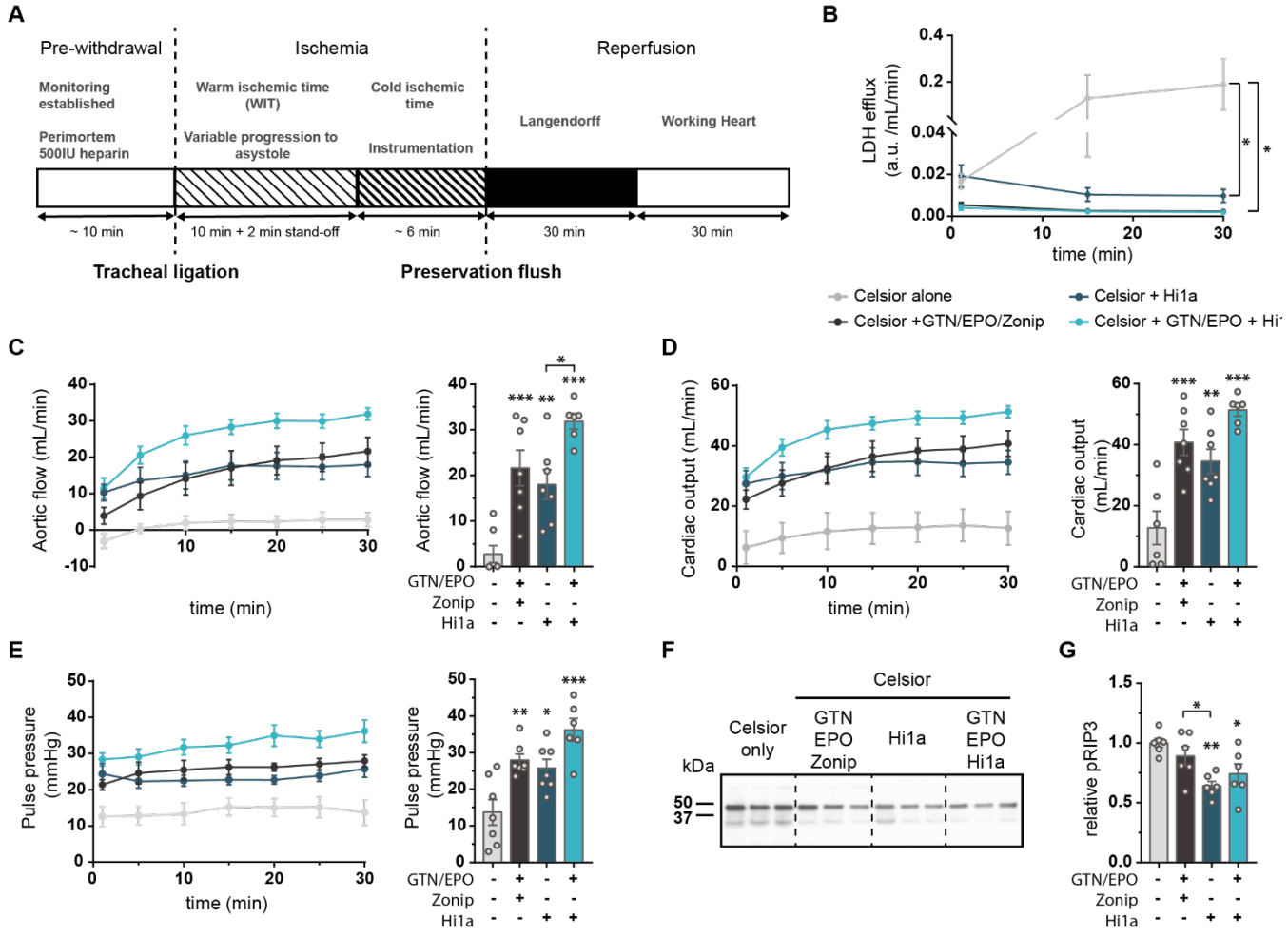

Figure 4. Hi1a protects rat hearts in a preclinical model of DCD. (**A**) Experimental design to mimic clinical DCD withdrawal. (**B-F**) Biochemical and functional characterisation of DCD hearts flushed with preservation solution (Celsior ± supplementation). (**B**) Arbitrary LDH units in the coronary effluent throughout 30 min working mode (normalized to coronary flow rate, LDH a.u./mL/min). (**C-E**) Assessment of heart function with (**C**) AF (mL/min), (**D**) CO (mL/min), and (**E**) PP (mmHg) plotted over time (left) and after 30 min in working mode (right). (**F**) Representative pRIP3 western blot on pRIP3-IP lysates collected at the end of reperfusion. Molecular masses as determined by BIO-RAD Precision Plus Protein ladder, are indicated on the left. Individual lanes represent different hearts (n = 6 hearts/group with 3 hearts/group/membrane). (**G**) Quantification of pRIP3 relative signal intensity (upper band, ~46 kDa), normalized internally to Celsior-only control. All data are expressed as mean ± SEM. For all experimental groups, n = 6–7 hearts. Statistical significance was determined using two-way (panel b) or one-way (panels c-g) ANOVA with multiple comparisons (*p < 0.05; **p < 0.01, ***p < 0.001).

conditions for 8 h, followed by reperfusion and functional analysis (**Figure 3A**). Hearts preserved with Hi1a supplementation had markedly improved recovery of aortic flow (AF) (50 ± 11%) and cardiac output (CO) (57 ± 8%) compared to Celsior-only controls (AF: 8 ± 5%; CO: 24 ± 5%) (**Figure 3B**,**C**). These data demonstrate that Hi1a is highly cardioprotective against IRI in a clinically relevant model of donor heart preservation with prolonged cold storage.

Hi1a supplementation improves recovery in a post-conditioning model of donation after circulatory death

To determine whether pharmacological inhibition of ASIC1a could recover hearts when delivered subsequent to a profound ischemic injury, we assessed the effect of Hi1a in a rodent model of donation after circulatory death (DCD)(*46*)·(*47-49*). To mimic a clinical DCD withdrawal for heart transplantation in rodents, asphyxiation was induced via tracheal ligation and the hearts were retrieved after a 10-min warm ischemic time (WIT) followed by 2-min stand-off period after cessation of circulation. Following ischemia, hearts were flushed with Celsior with or without supplementation, followed by *ex vivo* reperfusion in Langendorff mode for 30 min and then working mode for an additional 30 min (**Figure 4A**).

Hi1a (10 nM) was tested as a single supplement and in combination with two clinically used supplements, glyceryl trinitrate (GTN) and erythropoietin (EPO)(*49*).

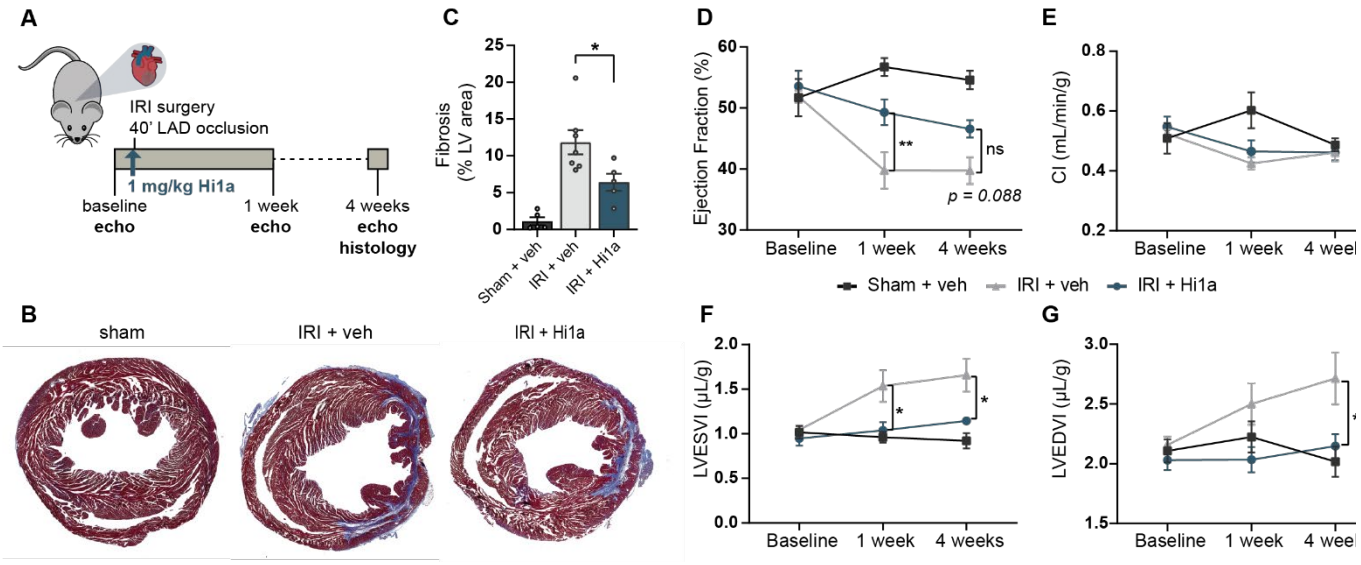

Figure 5. Hi1a protects post-ischemic cardiac remodelling after IRI *in vivo.* (**A**) Schematic of experimental design. (**B-C**) Mason's trichrome staining of heart sections at 28 days post injury. (**B**) Representative images of sham, vehicle-treated, and Hi1a-treated hearts depicting healthy myocardium (red) and collagen deposition/fibrosis (blue). (**C**) Quantification of fibrosis as a percentage of left ventricular area. (**D-G**) Functional parameters including ejection fraction (**D**) cardiac index (**E**), as well as LV end systolic (**F**) and diastolic (**G**) internal volume measured by serial echocardiography at baseline, 1 week, and 4 weeks post injury. All data are expressed as mean ± SEM (n = 5–7/group). Statistical significance was determined using one-way (panel c) or two-way repeated measures (panels d-g) ANOVA with multiple comparisons (*p < 0.05; **p < 0.01, ***p < 0.001).

As a positive control, we also evaluated zoniporide (Zon) combined with GTN and EPO, which we have previously shown activates ischemic postconditioning pathways through inhibition of NHE activity(*48*). To assess the viability of hearts post-DCD withdrawal, functional parameters and cell death (LDH release) were measured throughout working-mode reperfusion. In Celsior-only controls, coronary effluent levels of LDH increased throughout the 30 min assessment period. Allografts supplemented with Hi1a, Hi1a + GTN/EPO, or GTN/EPO/Zon, however, had significantly reduced levels of LDH after 30 min, with LDH release in both triple-supplemented groups comparable to a heart at baseline, prior to ischemic insult (**Figure 4B**). Functional parameters of recovery including AF, CO, and pulse pressure (PP) were all significantly improved in supplemented groups compared to Celsior alone (**Figure 4C-E**). AF, in particular, was significantly increased in hearts supplemented with Hi1a combined with GTN and EPO (32 ± 2 mL/min) compared to Hi1a as a single supplement (18 ± 3 mL/min), suggesting an additive effect of Hi1a with current clinically used cardioprotective agents (**Figure 4C**).

To investigate the therapeutic benefit of Hi1a in the context of preventing cell death in DCD hearts, we performed western blots to examine the levels of phosphorylated RIP3 (pRIP3) in tissue lysates collected at the end of working-mode reperfusion. RIP3 is a key regulator of the necroptosis pathway that has been implicated in the response to IRI(*50, 51*), and specifically to ASIC1a-mediated cell death during cerebral ischemia(*52*). Treatment with Hi1a as a single or triple supplement reduced the level of pRIP3 following DCD withdrawal and reperfusion (**Figure 4F**), suggesting that Hi1a blockade of ASIC1a might inhibit necroptosis. Together with our finding that Hi1a improved donor organ viability after prolonged cold storage, the therapeutic efficacy of Hi1a in the DCD model demonstrates significant translational potential for ASIC1a-targeted therapies during clinical donor heart preservation.

ASIC1a blockade prevents adverse chamber remodelling and improves cardiac function post IRI in vivo

We next evaluated whether Hi1a treatment improves recovery of function *in vivo* in a murine model of myocardial IRI (**Figure 5**). We carried out a preconditioning model in which Hi1a was delivered by bolus intravenous injection (1 mg/kg) in mice just prior to anaesthesia (**Figure 5A**). Mice were anaesthetised and intubated followed by surgical thoracotomy to enable ligation of the proximal left anterior descending (LAD) coronary artery. Cardiac ischemia was induced for 40 min followed by reperfusion. Mice were evaluated by serial echocardiography over 4 weeks to assess functional recovery, and terminal histological analysis of hearts was performed to examine fibrosis. At four weeks, analysis of fibrosis measured by Mason's trichrome as a percent of the left ventricle showed significant reduction in collagen deposition in Hi1a-treated hearts compared to vehicle-treated animals (**Figure 5B-C**). Histological data were supported by assessment of functional performance. As expected, vehicle treated animals showed significant

dilation of ventricular volumes at end systole and diastole with a concomitant decrease in ejection fraction compared to sham animals (**Figure 5D-G**). In contrast, ejection fraction was improved at one week in Hi1a-treated animals compared to vehicle controls, demonstrating a therapeutic functional benefit during the early remodelling phase that remained improved, albeit not significant, at 4 weeks ($p = 0.08$) (**Figure 5D**). Hi1a-treated hearts also showed no significant difference in ventricular volumes compared to sham at four weeks post-IRI, demonstrating that ASIC1a blockade prevents adverse myocardial remodelling post MI (**Figure 5F-G**). This preconditioning *in vivo* model provides evidence of efficacy by pharmacological blockade of ASIC1a, resulting in significantly improved cardiac geometry and function post IRI.

ASIC1 is expressed in the human heart and polymorphisms in its genetic locus are associated with ischemic disease

To assess conservation of ASIC1a biology in humans, we analysed ASIC expression patterns from mRNA-seq and ribo-seq data collected from human left ventricular cardiac tissue,(*53*) which revealed highest expression of *ASIC1* and *ASIC3* in the human left ventricle and similar levels of *ASIC1* expression in samples from HF and non-HF patients (**Supplemental Figure 3A**,**B**). We next assessed whether natural variation in the genetic locus encoding ASIC1a (*ACCN1*) is associated with ischemic diseases using human population statistical genetics. While fewer than 10% of new molecular entities that pass through clinical trials are approved for therapeutic use, evidence of human genetic association between the gene target and traits sufficiently similar to the indication being treated increases the likelihood of approval to as high as 50%(*54*). We utilized summary data from genome-wide association studies (GWAS)(*4*) and calculated the statistical significance (using fastBAT (*55*)) of genetic variants encompassing the *ACCN1* locus with human cardiac and cerebral ischemic phenotypes. These data revealed a significant association between genetic variation in *ACCN1* and major coronary heart disease and MI ($P < 0.05$) (**Table 2**). We also found that genetic variation in *ACCN1* associates with small-vessel ischemic stroke ($p = 3.94 \times 10^{-3}$), but not other stroke subtypes (**Table 2**). Taken together, these data provide evidence that *ACCN1* polymorphisms within the human population are associated with ischemic diseases of the heart and brain.

ASIC1a inhibition prevents cell death in in vitro human models of IRI

To examine whether pharmacological blockade of ASIC1a might provide therapeutic benefit in the context of human tissue, we used human induced pluripotent stem cell-derived cardiomyocytes (hiPSC-CMs). Contractile cardiomyocytes were generated from stem cells using a standard monolayer-based differentiation protocol involving bi-phasic Wnt regulation (**Figure 6A** and **Supplemental Figure 3C**). Analysis of mRNA transcripts from single-cell RNA sequencing data over a time course of cardiac differentiation from pluripotency(*1*) revealed that *ASIC1*, *ASIC3*, and *ASIC4* expression increased starting in day-5 cardiac progenitor populations and peaked in day-15 definitive cardiomyocytes. *ASIC1* was the most highly expressed ASIC subtype, with expression levels comparable to other cardiac ion channels, such as TRPV1 and $Na_V1.5$ (**Figure 6 B-C**).

Since ASIC1a mediates influx of calcium in addition to sodium(*41*), we performed calcium imaging after acute addition of Hi1a and PcTx1 to assess whether ASIC1a inhibition alters physiological electromechanical coupling in cardiomyocytes. Replated hiPSC-CMs were loaded with a fluorescent calcium dye and calcium transients were recorded before and after peptide addition. Neither Hi1a nor PcTx1 altered calcium amplitudes or spontaneous beating rate at any evaluated concentration (**Figure 6D**). To further demonstrate safety of ASIC1a blockade, we performed industry-standard patch-clamp electrophysiology analysis to examine the effect of Hi1a on the major off-target cardiac ion channels

Table 2. Association of polymorphisms in *ACCN1* with ischemic conditions. *ACCN1* gene position: chromosome 12, start: 50451419, end: 50477405)

Genotype	No. of SNPs	SNP start	SNP end	χ^2 statistic	Mean p-value
Acute myocardial infarction [1]	75	rs11377593	rs2242507	152.45	1.4E-02
Major coronary heart disease excluding revascularizations [1]	75	rs11377593	rs2242507	199.11	1.8E-03
Myocardial infarction [1]	75	rs11377593	rs2242507	186.59	3.1E-03
Any stroke [2]	61	rs78972052	rs2242507	81.81	1.5E-01
Any ischemic stroke [2]	62	rs78972052	rs2242507	77.28	2.0E-01
Large artery stroke [2]	63	rs78972052	rs2242507	67.30	3.5E-01
Cardioembolic stroke [2]	61	rs78972052	rs2242507	71.63	2.5E-01
Small vessel stroke [2]	64	rs78972052	rs2242507	147.48	3.9E-03

The number of SNPs inside the *ACCN1* locus was used to calculate the χ^2 statistic and p-value. Source data: GWAS results from [1] UK Biobank from Neale Lab (*4*) or [2] Malik et al. (*5*).

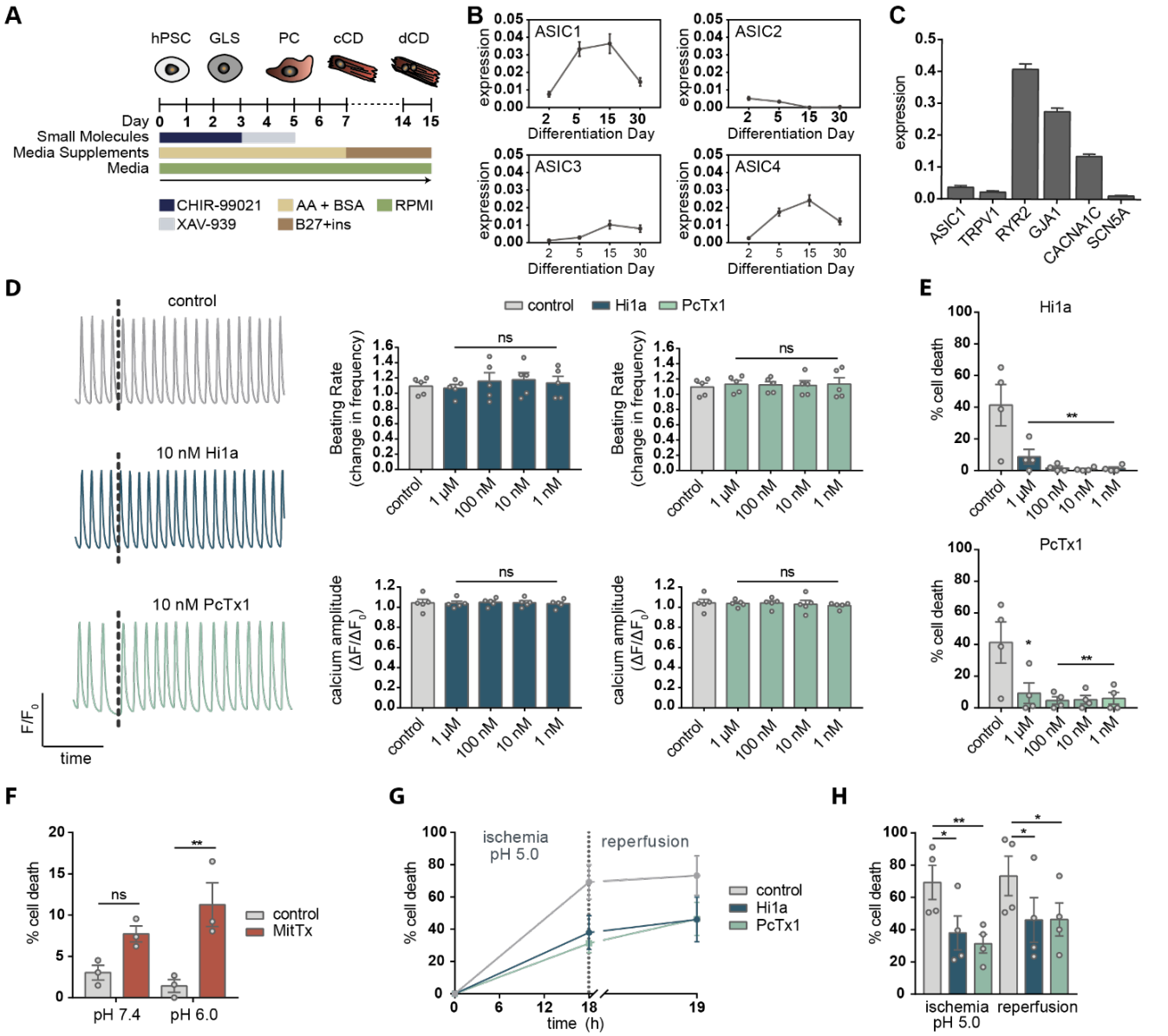

Figure 6. Hi1a protects hiPSC-CMs from ischemic injury. (**A**) Schematic depicting directed differentiation of hiPSC-CMs (adapted from Ref. (*1*)). (**B-C**) Analysis of published transcriptomic data (scRNAseq) of cardiac differentiation (*1*). (**B**) Expression of ASIC1, ASIC2, ASIC3, and ASIC4 at day 0, 2, 5, 15, and 30 of differentiation. (**C**) Gene expression in day-15 hiPSC-CMs. Abbreviations: RYR2 = ryanodine receptor 2; GJA1 = gap junction alpha1 protein (connexin 43). (**D**) Fluorescent imaging of calcium transients (normalized arbitrary fluorescent units (F/F_0)) before and after Hi1a or PcTx1 addition using a FLIPR Tetra system. Representative traces (black dotted line indicates time of peptide addition) and quantification of spontaneous beat rate and calcium amplitude are shown. Amplitude and beat rate are both expressed as a response over baseline (post-addition measurement normalized to pre-addition measurement). (**E**) Cell death (LDH secretion) analysis after overnight treatment in HBSS pH 5.0 with or without Hi1a (top) or PcTx1 (bottom). (**F**) Cell death (LDH) after overnight treatment with 20 nM MitTx in HBSS pH 7.4 or HBSS pH 6.0. (**G-H**) Cell death (LDH) after *in vitro* IRI with overnight hypoxic (0.5% O_2) incubation in HBSS pH 5.0 followed by 1 h reperfusion with HBSS pH 7.4 in normoxic conditions. For panels e–h, data are expressed as percent cell death calculated from LDH levels in low (RPMI + B27) and high (1% Triton X-100 in RPMI + B27) controls. All data are expressed as mean ± SEM (n = 3–5 biological replicates with 3–6 technical replicates each). Statistical significance was determined using one-way (panel d-e) or two-way (panel f, g) ANOVA with multiple comparisons (*$p < 0.05$; **$p < 0.01$).

(**Supplemental Table 1**). At 1 μM concentration, Hi1a had no major impact on $hNa_V1.5$, $hK_V4.3$/hKChIP2, $hCa_V1.2$, $hK_V11.1$/hERG, $hK_V7.1$/hKCNQ1, or hKir2.1 currents. Lastly, we showed that exposure of hiPSC-CMs to Hi1a for 48 h led to no significant alteration in cell viability compared to controls (**Supplemental Figure 3D**).

To assess whether ASIC1a inhibition is cardioprotective in hiPSC-CMs, we evaluated cell death in response to *in vitro* acidosis, induced by culturing hiPSC-

CMs in Hank's buffered sodium salt (HBSS) with pH adjusted to pH 7.4, 6.0, or 5.0. The requirement to expose cells to severe acidosis is consistent with previous studies showing reduced pH sensitivity in immature iPSC-derived cardiomyocytes(*56*) and is consistent with testing acid-sensitive ion channels *in vitro*(*57*). *ASIC1* mRNA expression was not significantly altered by low pH treatment, but significant cell death (> 40%), as assessed by LDH secretion, was observed in cultures treated overnight at pH 5.0, with minimal cell death occurring at pH 7.4 or pH 6.0 (**Supplemental Figure 3 E-F**). Treatment with either Hi1a or PcTx1 resulted in nearly complete cardioprotection, even at concentrations as low as 1 nM (**Figure 6E** and **Supplemental Figure 3 G-H**). To further confirm that ASIC1a plays a direct role in mediating cell death, we treated hiPSC-CMs overnight with 20 nM MitTx, a potent agonist of ASIC1a from snake venom(*58*). Consistent with ASIC1a mediating the injury response to cardiac ischemia, treatment of hiPSC-CMs with MitTx resulted in increased cell death at both pH 7.4 and pH 6.0 (**Figure 6F).** We next evaluated the cardioprotective effect of Hi1a and PcTx1 in an *in vitro* model of ischemia/acidosis with reperfusion. To mimic ischemia/acidosis *in vitro*, hiPSC-CMs were incubated overnight in combined hypoxic (0.5% O_2) and acidic (pH 5.0) conditions with or without peptide. After 18 h of incubation, the low-pH medium was replaced with medium at physiological pH 7.4 with or without peptide, and the cells were incubated for an additional hour under normoxic conditions. Significant cell death was observed in control hiPSC-CMs, but this was blocked by either 10 nM Hi1a or PcTx1 (**Figure 6 G-H**). These data suggest that ASIC1a mediates cell death responses in human cardiomyocytes and that pharmacological inhibition of ASIC1a confers significant protection against ischemia-induced cell stress.

Discussion

Despite decades of research and promising preclinical data, no pharmacological strategies have led to robust improvement in clinical outcomes for ischemic injuries of the heart(*16*). In this study, we show that ASIC1a significantly exacerbates myocardial injury responses to ischemia. Our findings are consistent with studies showing a role for ASIC1a during organ ischemia(*2, 39, 40*), and demonstrate therapeutic applications of ASIC1a-targeted therapies in myocardial IRI.

Although ASICs, and in particular ASIC1a, are generally associated with the central and peripheral nervous systems(*59*), our expression analyses revealed that ASIC1 is present in both rodent and human cardiomyocytes, and is not differentially regulated at the transcriptional level as a result of cellular ischemia *in vitro* or *in vivo*(*6*). Our evidence of ASIC1 expression in the heart is supported by recent studies that identified ASIC-like currents in hiPSC-CMs(*60*) and rat cardiomyocytes(*32*). In neurons, there are several possible mechanisms by which ASIC1a activation leads to cell death including calcium overload(*61*), regulation of mitochondrial permeability transition (MPT) pores(*62*), and the initiation of necroptosis through direct interaction with, and activation of, RIPK1(*52*). ASIC1a-induced cell death has not previously been described in cardiomyocytes, but there is evidence that ASIC1a, along with TRPV1, mediates calcium influx in response to extracellular acidosis(*32*). Importantly, given the potential for ASIC1a to transport calcium, we showed that genetic ablation or pharmacological inhibition of ASIC1a does not alter normal electromechanical coupling in the heart *in vitro* or *in vivo*.

Given that drug targets with genetic evidence of disease association are twice as likely to succeed in clinical trials and lead to approved drug candidates(*54*), our GWAS analysis of the association between genetic variation in the *ACCN1* locus and ischemic disease points towards the translational potential of ASIC1a-targeted therapies. Such therapies have the potential to impact a broad scope of clinical applications since myocardial IRI is evident in many cardiovascular complications such as acute MI, out-of-hospital cardiac arrest (OHCA), cardiopulmonary bypass, and heart preservation for transplantation(*13*). Despite intensive research into therapies aimed at mitigating myocardial IRI in the context of acute MI, none have translated into clinical practice.

In general, there is a strong association and co-morbidity between stroke and cardiac arrest, with 88% of patients suffering some form of cardiovascular complication within four weeks of an ischemic stroke(*63*). Likewise, cardiac interventions, such as transcatheter aortic valve implantation (TAVI), can cause cerebrovascular complications(*64*). We previously used a rat model of ischemic stroke to show that a single dose of Hi1a (2 ng/kg i.c.v) dramatically reduced infarct size and improved neurological and motor performance even when administered up to 8 h after stroke onset(*2*). No other drugs have been shown to provide significant protection beyond 4 h after stroke onset(*65*). Thus, ASIC1a inhibitors might provide a potential major advantage for clinical use due to their ability to protect both the heart and the brain from IRI, which is particularly relevant for OHCA, for which there is both cardiac and cerebral manifestations.

ASIC1a-targeted therapies appear to have significant potential in heart transplantation applications. The predominant source of donor hearts is brain dead (BD) donors, but the recent introduction of DCD hearts has increased the donor pool(*49*). The viability of usable BD and DCD hearts, however, continues to be adversely affected by unavoidable injury to the heart that occurs during organ procurement and storage, as well as reperfusion injury in the recipient. Indeed, the relative risk of one-year morbidity is strongly correlated with organ ischemic time(*13, 66*). In general, primary graft dysfunction is a major risk for patients in the first 30 days after transplantation and accounts for 66% of patient deaths, of which 48% are due to IRI(*67*). Thus, there is an

unmet need for effective, early interventions that reduce injury to the graft and reduce the risk of primary graft dysfunction in the recipient. Our direct comparison between Hi1a as a post-conditioning agent and supplements in current clinical use provide strong evidence for the clinical utility of Hi1a for increasing the pool of viable donor hearts for transplantation.

NHE inhibitors showed promise as an intervention for improving ischemic tolerance of DCD hearts(*48, 68*), as well as in a number of other clinical indications of myocardial IRI including cardiac surgery(*69*). However, in a Phase III clinical trial (the EXPEDITION Trial) of the NHE inhibitor cariporide, cerebrovascular complications halted therapeutic development, despite promising clinical evidence that NHE inhibitors can be effective at reducing myocardial IRI(*28*). Our direct comparison between Hi1a and current clinical preservation supplements, as well as the NHE inhibitor zoniporide, provide strong evidence for the clinical utility of ASIC1a inhibitors.

Venom-derived molecules have proven to be a source of novel therapeutics, particularly in the cardiovascular field. Examples include the antihypertensive drug captopril(*70*) derived from the venom of a Brazilian viper, and eptifibatide and tirofiban, antiplatelet drugs that are used to treat acute coronary syndromes(*71*). Disulfide-rich knottin peptides such as Hi1a are typically highly stable in biological fluids, and ziconitide, a knottin peptide derived from cone snail venom, is an FDA-approved analgesic(*71*). . In addition to its high stability, Hi1a is 170-fold more potent than a recently reported antibody against ASIC1a(*72*). For this reason, Hi1a is ideally suited for clinical use as an adjuvant to standard-of-care heart preservation solutions for heart transplant or in combination with mechanical procedures such as percutaneous coronary intervention for myocardial infarction.

In summary, we have shown that ASIC1a is a critical mediator of cell death during cardiac ischemia and that pharmacological inhibition of ASIC1a affords potent cardioprotection across rodent and human models of cardiac IRI. These findings suggest that ASIC1a inhibitors have the potential to significantly impact the public health burden of cardiovascular disease and result in improved outcomes for patients with cardiac ischemic injuries.

Materials and Methods

Study Design. All animal experiments were performed in accordance with protocols approved by the Animal Ethics Committee of The University of Queensland (UQ) (IMB/171/18) and Garvan Institute of Medical Research (16/38). All hiPSC studies were performed with consent from the UQ Institutional Human Research Ethics approval (HREC #2015001434). Additional information for each set of experiments, such as statistical analyses, exclusion criteria, and sample size, are detailed in the relevant methods section or figure legend. All data and materials associated with this study can be provided upon request.

Animals. All animals used in this study received humane care in compliance with Australian National Health and Medical Research Council guidelines and the *Guide for the Care and Use of Laboratory Animals* (U.S. National Institutes of Health). To test the therapeutic efficacy of ASIC1a inhibitors, male C57BL/6 mice (Langendorff IRI experiments) or male Wistar rats (donor organ preservation experiments) were purchased from the Animal Resource Centre (Canning Vale, Western Australia).

For genetic ablation studies, ASIC1a$^{-/-}$ mice were generated at the Australian Phenomics Facility. CRISPR/Cas9 technology was used to specifically target the mouse ASIC1a sequence. Use of guide RNAs (gRNA) with sequences CCGAGGAGGAGGAGGTGGGTGGT and GTACCATGCTGGGGAACTGCTGG resulted in single nucleotide deletions within both targeted regions, at positions 22 and 341 (NM_009597.2(ASIC1_v001):c.22del and NM_009597.2(ASIC1_v001):c.341del). These deletions predicted a disrupted ASIC1a protein sequence (p.Glu8Argfs*9 and p.Leu114Argfs*94, respectively). The founder mouse was backcrossed to C57BL/6 background. Both hetero- and homozygous mice were viable and showed no obvious phenotype. Total RNA was isolated from brain tissue using Trizol Reagent (ThermoFisher Scientific, Massachusetts, USA), and contaminant genomic DNA was removed with DNA-free reagents (Ambion/Life Technologies, Austin, USA). Primer sequences designed to distinguish between ASIC1a and ASIC1b transcripts were used to determine gene expression levels in ASIC1a KO and WT animals(*73*). Primer sequences used in this study were ASIC1a forward 5′-CTGTACCATGCTGGGGAACT-3′ and reverse 5′-GCTGCTTTTCATCAGCCATC-3′; ASIC1b forward 5′-TGCCAGCCATGTCTTTGTG-3′ and reverse 5′-CACAGGAAGGCACCCAGT-3’ and RPL32 (for sample normalization) forward 5’-GAGGTGCTGCTGATGTGC-3’ and reverse 5’-GGCGTTGGGATTGGTGACT-3’. For quantitative real-time (qRT)-PCR, oligo-dT primed cDNA was synthesized from 500 ng of total RNA using Murine Moloney Leukaemia Virus reverse transcriptase (Promega, USA). qRT-PCR was performed using a ViiA Real-Time PCR System (Applied Biosystems, CA, USA) using SYBR green master mix (Promega, USA) according to manufacturer protocols. Relative ASIC1a and ASIC1b gene expression values were obtained from ASIC1a$^{-/-}$ mice and WT (ASIC1a$^{+/+}$) mice (calibrator) by normalization to the reference gene RPL32 using the 2-ΔΔCt method, where 2-ΔΔCt = ΔCt sample – ΔCt calibrator.

IRI in Langendorff-perfused mouse hearts. Isolated hearts were assessed for tolerance to IRI as previously described(*74, 75*). Mice (12–14 weeks) were anesthetized via an intraperitoneal injection of 10 mg/mL ketamine and

1.6 mg/mL xylazil. The heart was excised via thoracotomy and the aorta cannulated. The hearts were retrogradely perfused under constant hydrostatic pressure (80 mmHg) with oxygenated (95% O_2; 5% CO_2) modified Krebs-Henseleit buffer (composition in mM: 119 NaCl, 22 $NaHCO_3$, 4.7 KCl, 1.2 $MgCl_2$, 1.2 KH_2PO_4, 0.5 EDTA, 1.85 $CaCl_2$, 11 D-(+)-glucose, 2 Na^+ pyruvate, all from Sigma-Aldrich). Temperature was continuously measured with thermocouple needle microprobes (SDR Scientific) and maintained at 37°C with circulating water baths. Contractile function was measured via a fluid-filled balloon inserted in the left ventricle and connected to a pressure transducer (ADInstruments Pty Ltd.). Coronary flow was measured with an in-line Doppler flow probe positioned above the aortic cannulae (Transonic Systems Inc.). All functional data were recorded on a four-channel MacLab system (ADInstruments Pty Ltd.). Following 15–30 min of equilibration, hearts were switched to ventricular pacing at 420 beats/min (BPM) using a SD9 stimulator (Grass Instruments, Inc.). Baseline measurements were made for 10–20 min followed by 25 min of global normothermic ischemia and 45 min of reperfusion. Pacing was stopped during ischemia and resumed after 15 min of reperfusion. For peptide-treated experimental groups, 1 μM peptide solution was infused with a syringe pump (World Precision Instruments, LLC.) into the buffer, directly upstream of the cannula, at a rate of 1% of CF, for a final working concentration of 10 nM. Peptide was infused for 10 min prior to the onset of ischemia and during the first 15 min of reperfusion. To assess cell death, effluent was collected at 2 and 45 min after the start of reperfusion. Effluent levels of LDH were measured using a cytotoxicity detection kit (Roche). Normalized absorbance values (absorbance at 492 nm minus absorbance at 690 nm) were measured using a PHERAStar FS microplate reader (BMG Labtech). Standard curves were generated with bovine LDH (Sigma-Aldrich) and used to convert sample absorbance values to units of LDH. Data were normalized to CF and heart weight and then expressed as U/min/g. For all analyses, hearts were excluded if they met the following criteria: abnormally high coronary flow (> 8 mL/min), delayed onset of ischemic contracture (time to onset of ischemic contracture (TOIC) > 20 min), poor contractile function after equilibration (significant arrhythmias and/or left ventricular systolic pressure < 80 mmHg), or technical issues with the perfusion rig.

Isolated working model of donor heart preservation after prolonged cold storage. The isolated working heart model of donor heart preservation has been previously described(*76-78*). Male Wister rats (325–395 g) were anesthetized with an intraperitoneal injection of ketamine (80 mg/kg; Cenvet, Australia) and xylazine (10 mg/kg; Provet, Australia), with supplemental doses given as necessary until adequate anaesthesia was achieved. An incision was made in the abdomen of the animal and a bolus injection of 300 IU of heparin administered into the renal vein. A sternotomy was performed and the heart was excised and arrested by immersion in ice-cold Krebs-Henseleit buffer (composition in mM: 118 NaCl, 4.7 KCl, 1.2 $MgSO_4$, 1.2 KH_2PO_4, 25 $NaHCO_3$, 1.4 $CaCl_2$, 11 glucose, all from Sigma-Aldrich). Following aortic cannulation, hearts were stabilised for 10 min by retrograde (Langendorff) perfusion with Krebs-Henseleit buffer (37°C), at a hydrostatic pressure of 100 cm H_2O. During this period, the left atrial appendage was cannulated. This nonworking Langendorff system was converted to a working preparation by switching the supply of perfusate from the aorta to the left atrial cannula at a hydrostatic pressure of 15 cm H_2O (preload). The working heart ejected perfusate into the aortic cannula against the maintained fixed hydrostatic pressure of 100 cm H_2O (afterload). Aortic pressure was monitored via a side arm of the aortic cannula with a pressure transducer (Ohmeda, Pty Ltd., Singapore). AF was measured by an in-line flowmeter (Transonics Instruments Inc., Ithaca, NY). Aortic pressure and flow were recorded using PowerLab/4e (ADInstruments Pty Ltd, Sydney, Australia) with heart rate (HR) calculated from the flow trace. CF was measured by timed collection of effluent draining from the heart via a small incision in the pulmonary artery. CO was calculated from the sum of AF and CF. The hearts were maintained in working mode for 15 min, at which time functional parameters (AF, CF, CO and HR) were recorded and defined as the baseline value. Any hearts having a baseline AF < 35 mL/min, HR < 200 bpm, or CF < 10 mL/min were excluded at this stage. The heart was arrested by infusion of a preservation flush containing Celsior solution (2–3°C) ± 10 nM Hi1a via the aortic cannula (60 cm H_2O infusion pressure over 3 min), immersed in 100 mL Celsior ± 10 nM Hi1a, and kept on ice for 8 h. The heart was remounted on the perfusion apparatus and perfused with fresh Krebs-Henseleit buffer for 15 min in Langendorff mode, followed by 30 min in working mode. Celsior solution was obtained from the Institut Georges Lopez (Lissieu, France). Cardiac functional indices after 30 min of working-mode reperfusion were expressed as percent recovery of baseline values.

Donor heart preservation following circulatory death in rodents. The rodent DCD model (**Figure 4A**) was developed by our laboratory to closely mimic the events during withdrawal of life support (WLS) in the clinical scenario. Male Wister rats (325–395 g) were anesthetized with an intraperitoneal injection of ketamine (80 mg/kg; Cenvet, Australia) and xylazine (10 mg/kg; Provet, Australia), with supplemental doses given as necessary until adequate anaesthesia was achieved. Non-invasive monitoring was established, consisting of measurement of pulse oximetry (Rad-5v, Masimo Inc., Irvine, CA) and continuous electrocardiogram (P55 AC pre-amplifier, Grass Instrument Co., RI). A midline incision was made in the neck of the animal to expose the right carotid artery, which was cannulated for invasive monitoring of arterial

pressure via a pressure transducer (Ohmeda, Pty Ltd., Singapore). Once baseline monitoring parameters were recorded, a dose of 500 IU for antemortem heparin was delivered via a side port in the arterial pressure monitoring line. The animal was subjected to WLS via asphyxiation. A fixed warm ischemic time of 10 min followed by a 2-min stand-off period was chosen to mimic Australian federal regulations regarding DCD heart retrieval(*49*). Upon completion of the stand-off period, the heart and lungs were swiftly excised *en bloc* and immersed in ice-cold Krebs-Henseleit buffer. The aorta and left atrium were fashioned for instrumentation on an *ex-vivo* Langendorff perfusion apparatus. Once the aorta was cannulated onto the *ex-vivo* circuit, the pulmonary veins were rapidly ligated, and the preservation flush (Celsior solution (2–3°C) ± supplements) was commenced via the aortic cannula at a flow rate of 15–20 mL/min up to a total volume of 100 mL. The following concentrations of supplements were used: Hi1a: 10 nM; GTN: 100 mg/L; EPO: 5 U/mL; zoniporide: 1 µM. Left atriotomy was performed to prevent left ventricle distension and to facilitate cannulation on the *ex-vivo* apparatus for functional assessment during the working phase of the experiment.

Following the preservation flush, Langendorff reperfusion was commenced for a period of 30 min, using oxygenated Krebs-Henseleit buffer (37°C) to allow stabilization and recovery of the heart. As previously described, the apparatus was converted to a working mode via switching the supply of perfusate from the aortic to the left atrial cannula at a hydrostatic pressure of 15 cm H_2O (preload). Functional parameters (AF, CO, PP and HR) were measured continuously, and CF measured at 5-min intervals, during working mode. Left ventricular free-wall samples were collected at the end of the experiment for additional analysis via western blot (see supplemental methods). To assess cell death throughout reperfusion, coronary effluent samples were collected at 1, 15, and 30 min of working mode and LDH levels were measured using the TOX 7 assay kit (Sigma-Aldrich). Duplicate 75-µL aliquots were assayed according to the manufacturer's instructions. The resulting absorbance of the tetrazolium product was measured at 492 nm using a 96-well plate reader and expressed as arbitrary units, normalised to coronary flow per minute.

Proteomics: Frozen ventricular tissue (50 mg) was pooled on dry ice from 3 biological replicates on two separate occasions (n=6 biological replicates) before protein extraction, as previously described with minor modifications(*79*). Briefly, myocardial samples were homogenised in 3 volumes of homogenisation buffer (6 mol/L urea, 2 mol/L thiourea) containing protease inhibitors (1 µmol/L aprotinin, 1 µmol/L pepstatin A, 1 µmol/L leupeptin, 1 µmol/L phenylmethylsulphonyl fluoride [PMSF]) by 2 rounds x 10 sec hand-held homogenising (Omni, Kennesaw GA) and 1 round x 20 sec bead-beating (MPbio, Irvine, CA). The homogenate was cleared of cellular debris by centrifugation at 14000 x *g* for 15 min at 6°C. Proteins were precipitated in 4 volumes of acetone overnight at -30°C, resolubilised in homogenisation buffer then reduced and alkylated with 10 mmol/L dithiothreitol (DTT) and 20 mmol/L iodoacetamide (IAA), respectively; prior to digestion in 50 mmol/L HEPES (pH 7.6) for 24 hours at 26°C with sequencing grade trypsin (1:33 trypsin: protein; Promega, Madison WI). The digests were acidified to 1% trifluoroacetic acid (TFA) prior to desalting and concentration by hydrophilic-lipophilic balance (HLB) chromatography (Waters, Bedford MA). Peptides were reconstituted in 50 mmol/L HEPES and adjusted to pH 8.5 before fluorometric quantitation (Qubit; Thermo Fisher Scientific). For relative quantitation, a volume containing 50 µg peptide was aliquoted from each biological condition, for labelling with 0.16 mg tandem mass tags (TMTsixplex; Thermo Fisher Scientific) according to the manufacturer's instructions (Table X). The biological groups were pooled and desalted by HLB as above. TMTsixplex labelled samples were fractionated offline by reverse phase C-18 liquid chromatography (RP-LC) using an Agilent 1200 LC system (Agilent Technologies, Santa Clara CA). Samples were loaded onto a 15 cm x 300 µm column packed in-house with 3.5 µm X-Bridge C18 particles (Waters Corp, Milford MA) in 100% buffer A (10mM ammonium formate, pH 7.9) for 10 min at 10 µL/min. Peptides were eluted over a 40 min linear gradient spanning 10-60% buffer B (0.1% TFA) at 6 µL/min with fractions collected at 1 min intervals. Mid pH fractions were concatenated into 12 fractions for before liquid chromatography-tandem mass spectrometry (LC-MS/MS) with separation by reverse phase chromatography (C18, 1.9 µm particle size; Dr Maisch, Ammerbuch, Germany) on an in-house 40 cm x 75 µm column with integrated emitter across a gradient of 5%-35% acetonitrile (MeCN) with 0.1% formic acid (FA) over 90 min at 300 nL/min using a Dionex UltiMate 3000 UHPLC coupled to a Q-Exactive HF-X mass spectrometer (Thermo Fisher Scientific), as previously described(*80*). Data were acquired in positive polarity, and the instrument operated in data dependant acquisition mode (DDA), with MS1 scans acquired from 300-1650 *m/z* (60000 resolution, 3e6 automatic gain control [AGC], 50 msec injection time), followed by 20 MS/MS scans performed using higher-energy collisional dissociation (HCD) fragmentation (0.7 *m/z* isolation window, 15000 resolution, 1e5 AGC, 30 normalised collision energy [NCE]).

Data were processed with Proteome Discoverer v.2.4 against the Mus Musculus (WT vs KO) UniProtKB/Swiss Prot database (October 2019; 25,096 entries), using an in-house Mascot (Matrix Science, UK) server. Searches were performed using up to 2 missed cleavages, mass tolerance 20 ppm (MS1) and 0.2 Da (MS2), variable modifications (oxidation (Met), acetylation (Protein *N*-termini), deamidation (Asn and Gln)) and fixed modifications (TMTsixplex (peptide *N*-termini and Lys) and

carbamidomethyl (Cys)). Peptide level false discovery rate (FDR) was determined using Percolator (v. 2.08.01) and all searches were filtered for <1% FDR, peptide length between 6-40 residues and rank 1 peptide identifications. Samples were normalised using median signal intensity, with median log2 ratios calculated at the peptide and protein level within each biological replicate. A minimum of 2 peptides per protein were required for confident identification and quantification of proteins. The weighted average log2 ratio was calculated across replicate experiments, with proteins deemed to be significantly regulated based on a zScore of ±1.00 and p-value <0.05.

In vivo myocardial IRI surgery. Surgeries were performed on 10-week-old male mice (C57BL/6). The surgeon was blinded to the treatments in all surgery. Prior to anaesthesia, mice were injected with 1 mg/kg Hi1a or vehicle control (0.1% BSA in saline) via tail vein injection. Mice were anesthetized by 4% isoflurane followed by endotracheal intubation and mechanical ventilation. Analgesia was provided by subcutaneous injection of buprenorphine (0.05 mg/kg). Isoflurane was reduced to 2 – 2.5% to maintain anaesthetic plane for the remainder of the procedure. A lateral thoracotomy was performed, the left anterior descending artery (LAD) identified and temporarily occluded (40 minutes of ischemia) 2 mm below the left atrial appendage with 7-0 prolene suture (Ethicon, Somerville, NJ, USA) tied around a piece of PE10 tubing placed on the LAD. Successful ligation was confirmed by significant blanching of the myocardium below the point of ligation. At the end of the ischemic period, the suture and tubing were removed and reperfusion was confirmed with returned pallor of the myocardium. After surgery, the chest and skin were closed with 5-0 prolene suture (Ethicon, Somerville, NJ, USA) and the mice allowed to recover. Sham operated mice underwent the same procedure without LAD ligation. Body temperature was controlled and monitored via a rectal probe for the duration of the surgery to maintain 37.0 ± 0.5°C. Buprenorphine (0.05 mg/kg) was administered every 12 hours for three additional days and the overall post-operative health of the animals were closely monitored every day.

Echocardiography

Echocardiography was performed prior to surgery (baseline), and at 1- and 4- weeks post-surgery using a Vevo3100 ultrasound system (VisualSonics, Toronto, Canada) with a 25 - 55 MHz transducer (MX550D). All echocardiographic measurement and analysis were conducted in a blinded manner. Mice were anesthetized with 2.5% isoflurane and general anaesthesia was maintained with 1% isoflurane during echocardiography. Mice in supine position were placed on a heating pad and heart rate (HR) and electrocardiography were recorded. Body temperature was controlled and monitored for the duration of the echocardiography to maintain 37.0 ± 0.5°C. Two-dimensional B-mode images were recorded in the parasternal long axis view and used to determine left ventricle end-diastolic volume (LVEDV), left ventricle end-systolic volume (LVESV), ejection fraction (EF), and cardiac output (CO). LVEDV, LVESV, and CO were normalized to body weight [left ventricle end-diastolic volume index (LVEDVI), left ventricle end-systolic index (LVESVI), and cardiac index (CI), respectively]. The recorded images were analysed using Vevo LAB 3.1.1 software (VisualSonics, Toronto, Canada). All parameters were measured at least three times and the averages are presented.

Histology.

At the experimental endpoint (4 weeks), the mice were euthanized with an overdose of ketamine (10 mg/mL ketamine) and xylazil (1.6 mg/mL). The hearts were perfused with 3–4 mL PBS via intracardiac injection followed by excision of the heart. The hearts were briefly submerged in supersaturated KCl (>5M) to arrest the heart in diastole followed by overnight fixation in 4% paraformaldehyde at 4°C. Samples were transferred to 70% EtOH and paraffin processed and embedded. 4 µm sections were cut and stained for Masson's trichrome blue. Stained sections were imaged at 10X resolution with a slide scanner (Zeiss Axioscan), and analysed with ZEN Lite 3.1. For each heart, the area of fibrosis (blue) was measured in 4 separate sections (2 mm tiles from apex to base) with ImageJ software. Values are presented as a summation of fibrosis area in all 4 sections divided by total LV area.

Peptide production. Recombinant Hi1a was produced by expression as a His_6-maltose-binding protein (MBP) fusion protein in the periplasm of *Escherichia coli* as previously described(*2*), but with optimisation of the expression and purification conditions to improve the yield. Briefly, *E. coli* BL21(DE3) cells were grown at 30°C in Terrific Broth until the optical density at 600 nm reached 2.0−2.5, at which point the temperature was reduced to 17°C and expression of the Hi1a fusion protein was induced with 1 mM IPTG. Cells were harvested after a further 21 h growth. PcTx1 and the PcTx1-R27A/V32A analogue were produced in the same manner with minor modifications to the expression protocol. *E. coli* were grown at 37°C for the entire expression period and harvested approximately 4−5 h after induction. Cell pellets were resuspended in 50 mM Tris, 300 mM NaCl, 5% glycerol, 15 mM imidazole (pH 8.3 for Hi1a or pH 8.0 for PcTx1), and the cells were lysed by high-pressure cell disruption (Constant Systems Limited, UK). The His_6-MBP-peptide fusion proteins were purified from the clarified soluble lysate over a nickel affinity resin. The resin was washed with the same buffer to elute weakly bound proteins before eluting the Hi1a fusion protein with the same buffer containing 300 mM imidazole. Fusion proteins were exchanged into low (< 30 mM) imidazole buffer using an Amicon Ultra-15 centrifugal concentrators (Merck Millipore, Germany) with a 30 kDa molecular

weight cut-off in preparation for liberation of Hi1a from the fusion tag using tobacco etch virus (TEV) protease. The fusion proteins were cleaved in redox buffer containing 3 mM reduced glutathione and 0.3 mM oxidised glutathione at pH 8.3 for Hi1a or pH 8.0 for PcTx1, using ~1 mg of TEV protease per 50 mg of fusion protein. For Hi1a the cleavage reaction was allowed to proceed at 4ºC over 3−6 days. For the PcTx1 peptides, cleavage was performed at room temperature for a minimum of 16 h. The recombinant peptides each contain a non-native N-terminal serine residue, which is a vestige of the TEV protease recognition site. The released peptides were purified from the cleavage reaction solutions using reverse phase high-performance liquid chromatography. The mass of the purified peptides were confirmed by electrospray-ionisation mass spectrometry and pure peptides were lyophilised prior to confirmation of ASIC1a inhibitory activity using two-electrode voltage-clamp electrophysiology, as described previously for Hi1a(*2*) and PcTx1(*3, 39, 81*). Unless otherwise noted, lyophilized stocks of peptide were reconstituted in sterile deionised water prior to use.

Generation of cardiomyocytes from hiPSCs. Cardiomyocytes generated in this study were derived from the WTC-11 hiPSC line (Gladstone Institute of Cardiovascular Disease, UCSF) (*82, 83*). Undifferentiated hiPSCs were maintained on Vitronectin XF (5 µg/mL, Stem Cell Technologies) coated tissue culture dishes as per manufacturer recommendation with either mTeSR or mTeSR PLUS medium with supplementation (Stem Cell Technologies). Contractile cardiomyocytes were differentiated using a high-density monolayer format as described(*1*). hiPSCs were dissociated with 0.5 mM EDTA solution supplemented with 1.1 mM D-glucose. Single-cell suspensions were plated at a density of 1.2 x 10^5 cells/cm^2 and cultured overnight in mTeSR medium supplemented with 10 µM Y-27632 dihydrochloride (Stem Cell Technologies). Once the monolayer reached approximately 80% confluence (usually the following day), differentiation was induced (day 0). The cells were quickly washed with PBS followed by a change in medium to RPMI (ThermoFisher) containing 3 µM CHIR99021 (Stem Cell Technologies), 500 µg/mL BSA (Sigma Aldrich), and 213 µg/mL ascorbic acid (Sigma Aldrich). After 3 days of culture, the medium was exchanged to RPMI containing 500 µg/mL BSA, 213 µg/mL ascorbic acid, and 5 µM Xav-939 (Stem Cell Technologies). On day 5, the medium was replaced with RPMI containing BSA and ascorbic acid as on day 3. Starting on day 7, the cells were fed every other day with RPMI containing 1x B27 supplement with insulin (Life Technologies). Spontaneous beating was typically observed between days 9 and 11 of differentiation.

In vitro *ischemia-acidosis injury model with hiPSC-CMs.* Differentiated cardiomyocytes were replated on either day 15 or day 17 of differentiation for *in vitro* ischemia/acidosis assays. At the time of replating, a subset of cells (~500,000) was set aside for flow cytometry analysis of cardiomyocyte purity (see supplemental methods). For all experiments, only cell preparations with > 80% sarcomeric α-actinin-positive cardiomyocytes were used. After re-plating, the cells were maintained for an additional 7 days in RPMI + B27. To prepare media for ischemia/acidosis injury, 10x HBSS without sodium bicarbonate (Sigma) was diluted to 1x concentration in sterile tissue culture-grade water. Solutions were buffered with either 12 mM HEPES (for pH 7.4 media, Sigma Aldrich) or 12 mM MES (for pH < 6.5, Sigma Aldrich) and the pH adjusted accordingly with 1 M NaOH. The medium was sterile filtered with 0.22 µm syringe filters (Millipore). Unless otherwise noted, the replated cells were treated overnight (18 h) in HBSS with or without peptide under either normoxic (~18.5% O_2; 5% CO_2) or hypoxic (0.5% O_2; 5% CO_2) culture conditions. For reperfusion experiments, the medium was replaced with HBSS pH 7.4 (with or without peptide) after overnight incubation and cultured for 1 h under normoxic conditions. To assess cell death, supernatant was collected and LDH levels were measured using a cytotoxicity detection kit (Roche). For all cell culture experiments, percent cell death was calculated using low and high controls. For low control (LC), cardiomyocytes were cultured overnight in standard culture media (RPMI + B27). For high control (HC), cells were cultured in RPMI + B27 containing 1% Triton X-100 (Sigma-Aldrich).

hiPSC-CM calcium analysis. Cardiomyocytes were replated (2 x 10^4 per well) in 384-well plates (CellBIND black with clear bottom, Corning) and cultured for 7 days in RPMI + B27. On the day of the experiment, the cells were loaded for 1.5 h at 37°C with FLIPR calcium 4 dye (Molecular Devices) diluted in HBSS pH 7.4. After loading, the plate was transferred to a FLIPR Tetra fluorescent plate reader (Molecular Devices). Calcium transients were measured with excitation wavelengths at 470–495 nm and emission at 515–575 nm. For each plate, the camera gain and intensity were adjusted to optimize signal intensity. Data for each well were expressed as normalized arbitrary fluorescence units. All data were acquired at 0.5 s per read, with baseline measurements for 45 s followed by at least 100 s of data collection after each peptide addition. Peptide solutions (in HBSS pH 7.4) were added to each well to give a final concentration of 1 nM, 10 nM, 100 nM, or 1 µM. Calcium amplitude, maximum calcium, minimum calcium, and spontaneous beating rate were analysed using ScreenWorks software (Molecular Devices) and normalized to baseline measurements.

Analysis of GWAS studies. To assess whether genetic variation of *ASIC1* associates with cardiovascular disease and stroke, we performed a gene-based level test on GWAS summary data using fastBAT(*55*) implemented in the Complex-Traits Genetics Virtual Lab (CTG-VL)(*84*). GWAS summary data contains the statistical information

of the association of all the genetic variants included in a GWAS against a particular trait. fastBAT tests the aggregated effects of a set of genetic variants within or close to (± 50 kb) each tested gene (*ACCN1* in this case) using a set-based association approach which accounts for the correlation between genetic variants (i.e. linkage disequilibrium). This provides a more powerful approach over single-variant tests. Specifically, we performed analyses using GWAS summary data for acute MI (N_{cases} =5,948, $N_{controls}$ = 354,176), major coronary heart disease (N_{cases} = 10,157, $N_{controls}$ = 351,037) and MI (N_{cases} = 7,018, $N_{controls}$ = 354,176) from Neale's UK Biobank GWAS database(*4*) and stroke (including any type of stroke, ischemic stroke, large artery stroke, cardioembolic stroke and small vessel stroke(*5*) (N_{cases} =40,585, $N_{controls}$ = 406,111).

Statistical Analysis. All data are presented as mean ± SEM. Statistical analyses were performed with GraphPad Prism and comparisons were made using Student's *t*-test, one-way analysis of variance (ANOVA), or two-way ANOVA. All data were derived from a minimum of three independent experiments with specific information for each experiment detailed in the relevant figure legend. Differences were considered significant with $p < 0.05$.

Acknowledgements: We thank the Integrated Physiology Facility and Melanie Flint at UQ for technical support and assistance. Microscopy was performed at the Australian Cancer Research Foundation (ACRF)/Institute for Molecular Bioscience Cancer Biology Imaging Facility, which was established with support from ACRF. We gratefully acknowledge financial support from The University of Queensland (UQ) Strategic Funding Research Initiatives (to N.J.P., G.F.K., J.F.F., J.E.H., E.R.P., M.E.R., W.G.T.), the Australian National Heart Foundation (Grant 101889 to N.J.P.), NHMRC Development grant (2000178 to N.J.P, G.F.K, P.S.M and J.F.F) a Uniquest Pathfinder Award (N.J.P), the Whitaker International Program (Scholar Grant to M.A.R.), the American Australian Association (Grant 441 to M.A.R.), the St Vincent's Clinic Foundation (to P.S.M.), the Australian National Health & Medical Research Council (Program Grant 1074386 to P.S.M.; Project Grant APP1085996 to W.G.T.; Principal Research Fellowship APP1136889 and Development Grant APP1158521 to G.F.K.), and the Australian Research Council (Discovery Early Career Researcher Award DE180100976 to G.C.P.).

Author Contributions: M.A.R. designed, performed, and analysed the experiments presented in Figures 1, 2, 5, and 6, Table 1, and Supplemental Figures 1, 2, and 3, and wrote the manuscript. S.E.S. designed, performed, and analysed the experiments described in Figures 3 and 4 and wrote the manuscript. N.J.S. produced, purified, and performed QC analyses for peptides used in Figures 2 – 6 and Supplemental Figures 2 and 3. Y.Y. performed LAD occlusion surgery and echocardiography analysis presented in Figure 5. L.G., M.H., and J.E.V. helped design, perform, and interpret experiments described in Figures 3 and 4. M.E.R., W.G.T., J.N.P., J.Y.S., and L.E.S.H. conceived ideas and provided insights towards interpretation of results shown in Figures 1, 2, and 5. M.Y.W. and S.J.C. performed, analysed, and interpreted proteomics study in Figure 1 and Supplementary Figure 1. H.S.C. and X.C. helped perform the experiments described in Figure 5 – 6 and Supplemental Figure 3. M.A.H.A. helped perform the experiments described in Figures 1 and 2. Y.S. performed computational analysis presented in Supplemental Figure 3. J.E.H., G.A.Q., and E.R.P. generated data and analysed ASIC isoform expression in the heart in Figure 1A. G.C.P. performed GWAS analysis and interpretation presented in Table 2. J.F.F. helped conceive the heart transplant studies and provided intellectual and financial support. B.R., R.J.H., S.M., and S.P. generated and validated the ASIC1a knockout mouse strain used for studies presented in Figure 1 and Supplemental Figure 1. G.F.K. conceived of experimental objectives, provided intellectual and financial support, and directly supervised work related to peptide production utilized across all aspects of the study. P.S.M. conceived of experimental objectives, provided intellectual and financial support, and directly supervised work related to heart transplant modelling. N.J.P. conceived of experimental objectives, provided intellectual and financial support, and directly supervised work related to mouse IRI, GWAS analysis, human pluripotent stem cell modelling, and oversaw programmatic decisions regarding study design and completion in close collaboration with P.S.M. and G.F.K. All authors contributed to revisions and final preparation of the manuscript.

Sources of Funding: We gratefully acknowledge financial support from The University of Queensland (UQ) Strategic Funding Research Initiatives (to N.J.P., G.F.K., J.F.F., J.E.H., E.R.P., M.E.R., W.G.T.), the Australian National Heart Foundation (Grant 101889 to N.J.P.), the Whitaker International Program (Scholar Grant to M.A.R.), the American Australian Association (Grant 441 to M.A.R.), the St Vincent's Clinic Foundation (to P.S.M.), the Australian National Health & Medical Research Council (Program Grant 1074386 to P.S.M.; Project Grant APP1085996 to W.G.T.; Principal Research Fellowship APP1136889 and Development Grant APP1158521 to G.F.K.), and the Australian Research Council (Discovery Early Career Researcher Award DE180100976 to G.C.P.).

Disclosures: The authors have no conflicts of interest to disclose. All data and materials associated with this study can be provided upon request.

References

1. C. E. Friedman *et al.*, Single-Cell Transcriptomic Analysis of Cardiac Differentiation from Human PSCs Reveals HOPX-Dependent Cardiomyocyte Maturation. *Cell Stem Cell* **23**, 586-598.e588 (2018).
2. I. R. Chassagnon *et al.*, Potent neuroprotection after stroke afforded by a double-knot spider-venom peptide that inhibits acid-sensing ion channel 1a. *Proc. Natl. Acad. Sci. U.S.A.* **114**, 3750-3755 (2017).
3. N. J. Saez *et al.*, A dynamic pharmacophore drives the interaction between Psalmotoxin-1 and the putative drug target acid-sensing ion channel 1a. *Mol Pharmacol* **80**, 796-808 (2011).
4. . (The UK Biobank, http://www.nealelab.is/uk-biobank, 2018).
5. R. Malik *et al.*, Multiancestry genome-wide association study of 520,000 subjects identifies 32 loci associated with stroke and stroke subtypes. *Nat Genet* **50**, 524-537 (2018).
6. G. A. Quaife-Ryan *et al.*, Multicellular Transcriptional Analysis of Mammalian Heart Regeneration. *Circulation* **136**, 1123-1139 (2017).
7. Australian Institute of Health and Welfare, *National Hospital Mortality Database* (2018).
8. T. T. Cung *et al.*, Cyclosporine before PCI in patients with acute myocardial infarction. *N Engl J Med* **373**, 1021–1031 (2015).
9. V. L. Roger, Epidemiology of heart failure. *Circ Res* **113**, 646-659 (2013).
10. C. Cook, G. Cole, P. Asaria, R. Jabbour, D. P. Francis, The annual global economic burden of heart failure. *Int J Cardiol* **171**, 368-376 (2014).
11. J. P. Hellermann *et al.*, Heart failure after myocardial infarction: a review. *Am J Med* **113**, 324-330 (2002).
12. G. Savarese, L. H. Lund, Global Public Health Burden of Heart Failure. *Card Fail Rev* **3**, 7-11 (2017).
13. L. E. See Hoe, N. Bartnikowski, M. A. Wells, J. Y. Suen, J. F. Fraser, Hurdles to Cardioprotection in the Critically Ill. *Int J Mol Sci* **20**, E3823 (2019).
14. M. J. Kearns *et al.*, A Rodent Model of Cardiac Donation After Circulatory Death and Novel Biomarkers of Cardiac Viability During Ex Vivo Heart Perfusion. *Transplantation* **101**, e231-e239 (2017).
15. E. J. Benjamin *et al.*, Heart Disease and Stroke Statistics-2019 Update: A Report From the American Heart Association. *Circulation* **139**, e56-e528 (2019).
16. D. J. Hausenloy, D. M. Yellon, Ischaemic conditioning and reperfusion injury. *Nat Rev Cardiol* **13**, 193-209 (2016).
17. B. E. Sansbury *et al.*, Metabolomic analysis of pressure-overloaded and infarcted mouse hearts. *Circ Heart Fail* **7**, 634-642 (2014).
18. W. C. Stanley, F. A. Recchia, G. D. Lopaschuk, Myocardial substrate metabolism in the normal and failing heart. *Physiol Rev* **85**, 1093-1129 (2005).
19. C. M. Moon, Y. H. Kim, Y. K. Ahn, M. H. Jeong, G. W. Jeong, Metabolic alterations in acute myocardial ischemia-reperfusion injury and necrosis using in vivo hyperpolarized [1-(13)C] pyruvate MR spectroscopy. *Sci Rep* **9**, 18427 (2019).
20. J. Inserte *et al.*, High-fat diet improves tolerance to myocardial ischemia by delaying normalization of intracellular PH at reperfusion. *J Mol Cell Cardiol* **133**, 164-173 (2019).
21. A. A. Gorodetsky, I. A. Kirilyuk, V. V. Khramtsov, D. A. Komarov, Functional electron paramagnetic resonance imaging of ischemic rat heart: Monitoring of tissue oxygenation and pH. *Magn Reson Med* **76**, 350-358 (2016).
22. S. A. Gabel, H. R. Cross, R. E. London, C. Steenbergen, E. Murphy, Decreased intracellular pH is not due to increased H^+ extrusion in preconditioned rat hearts. *Am J Physiol* **273**, H2257-H2262 (1997).
23. S. M. Cobbe, P. A. Poole-Wilson, The time of onset and severity of acidosis in myocardial ischaemia. *J Mol Cell Cardiol* **12**, 745-760 (1980).
24. A. A. Gandhi, P. J. Akholkar, Metabolic acidosis in acute myocardial infarction. *International Journal of Advances in Medicine* **2**, 260-263 (2015).
25. S. Bhowmick *et al.*, Acidotoxicity via ASIC1a Mediates Cell Death during Oxygen Glucose Deprivation and Abolishes Excitotoxicity. *ACS Chem Neurosci* **8**, 1204-1212 (2017).
26. D. J. Conklin *et al.*, TRPA1 channel contributes to myocardial ischemia-reperfusion injury. *Am J Physiol Heart Circ Physiol* **316**, H889-H899 (2019).
27. H. El Banani, Changes in intracellular sodium and pH during ischaemia–reperfusion are attenuated by trimetazidine Comparison between low- and zero-flow ischaemia. *Cardiovasc Res* **47**, 688-696 (2000).
28. R. M. Mentzer, Jr. *et al.*, Sodium-hydrogen exchange inhibition by cariporide to reduce the risk of ischemic cardiac events in patients undergoing coronary artery bypass grafting: results of the EXPEDITION study. *Ann Thorac Surg* **85**, 1261-1270 (2008).
29. S. Vullo, S. Kellenberger, A molecular view of the function and pharmacology of acid-sensing ion channels. *Pharmacol Res*, 104166 (2019).

30. S. Gründer, X. Chen, Structure, function, and pharmacology of acid-sensing ion channels (ASICs): focus on ASIC1a. *Int J Physiol Pathophysiol Pharmacol* **2**, 73-94 (2010).
31. J. A. Wemmie, R. J. Taugher, C. J. Kreple, Acid-sensing ion channels in pain and disease. *Nat Rev Neurosci* **14**, 461-471 (2013).
32. Y. L. Hu *et al.*, Multiple H+ sensors mediate the extracellular acidification-induced [Ca(2+)]i elevation in cultured rat ventricular cardiomyocytes. *Sci Rep* **7**, 44951 (2017).
33. Z. Li *et al.*, TRPV6 protects ER stress-induced apoptosis via ATF6α-TRPV6-JNK pathway in human embryonic stem cell-derived cardiomyocytes. *J Mol Cell Cardiol* **120**, 1-11 (2018).
34. J. Lipski *et al.*, Involvement of TRP-like channels in the acute ischemic response of hippocampal CA1 neurons in brain slices. *Brain Res* **1077**, 187-199 (2006).
35. E. Babini, M. Paukert, H. S. Geisler, S. Grunder, Alternative splicing and interaction with di- and polyvalent cations control the dynamic range of acid-sensing ion channel 1 (ASIC1). *J Biol Chem* **277**, 41597-41603 (2002).
36. M. Li *et al.*, Acid-sensing ion channels in acidosis-induced injury of human brain neurons. *J Cereb Blood Flow Metab* **30**, 1247-1260 (2010).
37. D. C. Immke, E. W. McCleskey, Lactate enhances the acid-sensing Na+ channel on ischemia-sensing neurons. *Nat Neurosci* **4**, 869-870 (2001).
38. N. J. Allen, D. Attwell, Modulation of ASIC channels in rat cerebellar Purkinje neurons by ischaemia-related signals. *J Physiol* **543**, 521-529 (2002).
39. C. A. McCarthy, L. D. Rash, I. R. Chassagnon, G. F. King, R. E. Widdop, PcTx1 affords neuroprotection in a conscious model of stroke in hypertensive rats via selective inhibition of ASIC1a. *Neuropharmacology* **99**, 650-657 (2015).
40. Z. G. Xiong *et al.*, Neuroprotection in ischemia: blocking calcium-permeable acid-sensing ion channels. *Cell* **118**, 687-698 (2004).
41. E. L. Bassler, T. J. Ngo-Anh, H. S. Geisler, J. P. Ruppersberg, S. Grunder, Molecular and functional characterization of acid-sensing ion channel (ASIC) 1b. *J Biol Chem* **276**, 33782-33787 (2001).
42. L. M. Nielsen *et al.*, Efficacy and safety of PPC-5650 on experimental rectal pain in patients with irritable bowel syndrome. *Basic Clin Pharmacol Toxicol* **116**, 140-145 (2015).
43. Z. G. Zhang, X. L. Zhang, X. Y. Wang, Z. R. Luo, J. C. Song, Inhibition of acid sensing ion channel by ligustrazine on angina model in rat. *Am J Transl Res* **7**, 1798-1811 (2015).
44. A. Baron, E. Lingueglia, Pharmacology of acid-sensing ion channels - Physiological and therapeutical perspectives. *Neuropharmacology* **94**, 19-35 (2015).
45. P. Menasche *et al.*, Experimental evaluation of Celsior, a new heart preservation solution. *Eur J Cardiothorac Surg* **8**, 207-213 (1994).
46. P. S. Macdonald, Heart Transplantation From DCD donors: From the Bedside to the Bench. *Transplantation* **101**, 1753-1754 (2017).
47. A. Iyer *et al.*, Normothermic ex vivo perfusion provides superior organ preservation and enables viability assessment of hearts from DCD donors. *Am J Transplant* **15**, 371-380 (2015).
48. A. Iyer *et al.*, Increasing the tolerance of DCD hearts to warm ischemia by pharmacological postconditioning. *Am J Transplant* **14**, 1744-1752 (2014).
49. K. K. Dhital *et al.*, Adult heart transplantation with distant procurement and ex-vivo preservation of donor hearts after circulatory death: a case series. *Lancet* **385**, 2585-2591 (2015).
50. A. Linkermann *et al.*, Two independent pathways of regulated necrosis mediate ischemia-reperfusion injury. *Proc. Natl. Acad. Sci. U.S.A.* **110**, 12024-12029 (2013).
51. H. Zhu, A. Sun, Programmed necrosis in heart disease: Molecular mechanisms and clinical implications. *J Mol Cell Cardiol* **116**, 125-134 (2018).
52. Y. Z. Wang *et al.*, Tissue acidosis induces neuronal necroptosis via ASIC1a channel independent of its ionic conduction. *Elife* **4**, 1-21 (2015).
53. S. van Heesch *et al.*, The Translational Landscape of the Human Heart. *Cell* **178**, 242-260.e229 (2019).
54. E. A. King, J. W. Davis, J. F. Degner, Are drug targets with genetic support twice as likely to be approved? Revised estimates of the impact of genetic support for drug mechanisms on the probability of drug approval. *BioRxiv*, 513945 (2019).
55. A. Bakshi *et al.*, Fast set-based association analysis using summary data from GWAS identifies novel gene loci for human complex traits. *Sci Rep* **6**, 32894 (2016).
56. A. Hidalgo *et al.*, Modelling ischemia-reperfusion injury (IRI) in vitro using metabolically matured induced pluripotent stem cell-derived cardiomyocytes. *APL Bioengineering* **2**, 026102-026102 (2018).
57. J. Yang *et al.*, PAC, an evolutionarily conserved membrane protein, is a proton-activated chloride channel. *Science* **364**, 395-399 (2019).

58. C. J. Bohlen *et al.*, A heteromeric Texas coral snake toxin targets acid-sensing ion channels to produce pain. *Nature* **479**, 410-414 (2011).
59. T. Besson, E. Lingueglia, M. Salinas, Pharmacological modulation of Acid-Sensing Ion Channels 1a and 3 by amiloride and 2-guanidine-4-methylquinazoline (GMQ). *Neuropharmacology* **125**, 429-440 (2017).
60. X. H. Zhang, T. Saric, N. Z. Mehrjardi, S. Hamad, M. Morad, Acid-Sensitive Ion Channels Are Expressed in Human Induced Pluripotent Stem Cell-Derived Cardiomyocytes. *Stem Cells Dev* **28**, 920-932 (2019).
61. Y. Herrera *et al.*, σ-1 receptor modulation of acid-sensing ion channel a (ASIC1a) and ASIC1a-induced Ca2+ influx in rat cortical neurons. *J Pharmacol Exp Ther* **327**, 491-502 (2008).
62. Y. Z. Wang *et al.*, Intracellular ASIC1a regulates mitochondrial permeability transition-dependent neuronal death. *Cell Death Differ* **20**, 1359-1369 (2013).
63. S. Ghanekar, S. Corey, T. Lippert, C. V. Borlongan, Pathological links between stroke and cardiac arrest. *Chin Neurosurg J* **2**, (2016).
64. J. P. Fanning *et al.*, Neuron-Specific Enolase and Matrix Metalloproteinase 9 Signal Perioperative Silent Brain Infarction During or After Transcatheter Aortic Valve Implantation. *Am J Cardiol* **123**, 434-439 (2019).
65. M. Fisher, J. L. Saver, Future directions of acute ischaemic stroke therapy. *Lancet Neurol* **14**, 758-767 (2015).
66. J. Stehlik *et al.*, The Registry of the International Society for Heart and Lung Transplantation: 29th official adult heart transplant report--2012. *J Heart Lung Transplant* **31**, 1052-1064 (2012).
67. J. Kobashigawa *et al.*, Report from a consensus conference on primary graft dysfunction after cardiac transplantation. *J Heart Lung Transplant* **33**, 327-340 (2014).
68. L. Gao *et al.*, Critical role of the STAT3 pathway in the cardioprotective efficacy of zoniporide in a model of myocardial preservation - the rat isolated working heart. *Br J Pharmacol* **162**, 633-647 (2011).
69. R. M. Mentzer, Jr., R. D. Lasley, A. Jessel, M. Karmazyn, Intracellular sodium hydrogen exchange inhibition and clinical myocardial protection. *Ann Thorac Surg* **75**, S700-S708 (2003).
70. L. H. Opie, H. Kowolik, The discovery of captopril: from large animals to small molecules. *Cardiovasc Res* **30**, 18-25 (1995).
71. G. F. King, Venoms as a platform for human drugs: translating toxins into therapeutics. *Expert Opin Biol Ther* **11**, 1469-1484 (2011).
72. M. Qiang *et al.*, Selection of an ASIC1a-blocking combinatorial antibody that protects cells from ischemic death. *Proc. Natl. Acad. Sci. U.S.A.* **115**, E7469-E7477 (2018).
73. E. N. Hoagland, T. W. Sherwood, K. G. Lee, C. J. Walker, C. C. Askwith, Identification of a calcium permeable human acid-sensing ion channel 1 transcript variant. *J Biol Chem* **285**, 41852-41862 (2010).
74. L. E. See Hoe *et al.*, Regulation of the beta-Adrenergic Receptor Signaling Pathway in Sustained Ligand-Activated Preconditioning. *J Pharmacol Exp Ther* **369**, 37-46 (2019).
75. M. E. Reichelt, L. Willems, B. A. Hack, J. N. Peart, J. P. Headrick, Cardiac and coronary function in the Langendorff-perfused mouse heart model. *Exp Physiol* **94**, 54-70 (2009).
76. F. Gao, J. Zhang, F. Wang, X. Xin, D. Sha, Cyclosporin A-related cerebral venous sinus thrombosis: A case report. *Medicine (Baltimore)* **97**, e11642 (2018).
77. J. Gao *et al.*, Coupling between NMDA receptor and acid-sensing ion channel contributes to ischemic neuronal death. *Neuron* **48**, 635-646 (2005).
78. G. Kumarasinghe *et al.*, Improved heart function from older donors using pharmacologic conditioning strategies. *J Heart Lung Transplant* **35**, 636-646 (2016).
79. B. L. Parker *et al.*, Structural basis for phosphorylation and lysine acetylation cross-talk in a kinase motif associated with myocardial ischemia and cardioprotection. *J Biol Chem* **289**, 25890-25906 (2014).
80. J. A. Cain *et al.*, Proteomics Reveals Multiple Phenotypes Associated with N-linked Glycosylation in Campylobacter jejuni. *Mol Cell Proteomics* **18**, 715-734 (2019).
81. N. J. Saez *et al.*, Molecular dynamics and functional studies define a hot spot of crystal contacts essential for PcTx1 inhibition of acid-sensing ion channel 1a. *Br J Pharmacol* **172**, 4985-4995 (2015).
82. Y. Miyaoka *et al.*, Isolation of single-base genome-edited human iPS cells without antibiotic selection. *Nat Methods* **11**, 291-293 (2014).
83. F. R. Kreitzer *et al.*, A robust method to derive functional neural crest cells from human pluripotent stem cells. *Am J Stem Cells* **2**, 119-131 (2013).
84. G. Cuellar-Partida *et al.*, Complex-Traits Genetics Virtual Lab: A community-driven web platform for post-GWAS analyses. *BioRxiv*, 518027 (2019).
85. J. Schindelin *et al.*, Fiji: an open-source platform for biological-image analysis. *Nat Methods* **9**, 676-682 (2012).
86. M. I. Love, W. Huber, S. Anders, Moderated estimation of fold change and dispersion for RNA-seq data with DESeq2. *Genome Biol* **15**, 550 (2014).
87. H. Wickham, *ggplot2: Elegant Graphics for Data Analysis*. (Springer-Verlag, New York, 2016).

SUPPLEMENTAL MATERIAL

Supplemental Methods

pRIP3 immunoprecipitation and western blot. Left ventricular tissue samples (~60 mg) from hearts (N = 6/group) collected at the end of the DCD protocol were homogenized in ice-cold lysis buffer (150 mM NaCl, 50 mM Tris-HCl, 1% Triton X-100, 1 mM sodium orthovanadate, 1 mM glycerophosphate, 5 mM dithiothreitol (DTT), 15% Roche cocktail protease inhibitors; pH 7.4). Samples were centrifuged at 10,000 rpm (9,400 *g*) for 5 min at 4°C and the supernatant collected. The protein concentration of each lysate was measured using a Bradford assay kit (Pierce Biotechnology, Rockford, IL), with bovine serum albumin used as standard. In order to detect and enrich for pRIP3, immunoprecipitations (IP) were performed on equal amounts of total protein from each sample. Lysate samples from individual hearts were centrifuged for 10 min at 10,000 *g* (4°C) and diluted with lysis buffer without DTT to make a final volume of 0.5 mL containing 1 mg of total proteins (1 µg/µL). Pre-clearing of the samples was performed by adding 60 µL of 50% Protein A agarose beads to 1 mL of diluted lysate from above. Samples were tumbled for 30 min at 4°C in a tube rotator, prior to being centrifuged for 5 min at 1,000 *g* (4°C), and supernatants were collected for immunoprecipitation. The cleared lysates were divided into two 400-µL aliquots and 1:100 specific primary antibody added to form the Ag/Ab complex (pRIP3 Ser227, Cell Signalling Technology, USA). 50 µl of 50% Protein A beads were added followed by gentle rocking for 2 h at 4°C. Following centrifugation for 30 s at 10,000 *g*, 4°C, the supernatant (containing unbound proteins) was discarded. The remaining pellet was washed five times with 500 µL of ice-cold lysis buffer. For each wash, the beads were re-suspended by inversion and centrifuged for 30 s at 1000 *g* at 4°C, prior to the supernatant being aspirated and discarded. The final pellet was resuspended with 50 µL of 2 x Laemmli sample loading buffer without β-mercaptoethanol. The samples were mixed vigorously and heat denatured for 5 min at 95°C. Following a 30 s centrifugation at 10,000 *g*, the supernatants were transferred to new vials and β-mercaptoethanol was added. The prepared samples were electrophoretically separated on 4–20% graduated precast gels (Bio-Rad) and transferred to polyvinylidene difluoride membranes. After blocking with 5% non-fat dry milk in Tris-buffered saline (TBS) containing 0.1% Tween-20, membranes were incubated overnight at 4°C with primary antibody (pRIP3 Ser227, Cell Signalling Technology, USA). Membranes were incubated with secondary anti-rabbit (1:2000 in 5% non-fat dry milk + TBS-T) or anti-mouse (1:5000 in 1% BSA + TBS-T) IgG conjugated to horseradish peroxidase (GE healthcare, Ryadalmere, Australia) for 1 h at 25°C. Protein bands were visualized using SuperSignal West Pico Chemiluminescent Substrate (Life Technologies, Scoresby, VIC, Australia), digitized, and quantified using Image J software (Version 1.52a, National Institute of Health, USA). Within each blot, the signal intensity from each lane was normalized to the Celsior-only group average from the same membrane. Blots were repeated to confirm results. All antibodies, unless otherwise stated, were sourced from Cell Signalling Technology (Beverly, MA).

Flow cytometry. To assess the cardiomyocyte purity of differentiated cell populations, cells were fixed with 4% paraformaldehyde (Sigma Aldrich), permeabilized in 0.75% saponin (Sigma Aldrich), and labelled with Phycoerythrin (PE)-conjugated sarcomeric α-actinin (SA) antibody (Miltenyi Biotec Australia Pty) or PE-conjugated mouse isotype (IgG) control (Miltenyi Biotec Australia Pty). Stained samples were analysed on a FACS CANTO II (Becton Dickinson) machine with FACSDiva software (BD Biosciences). Data were analysed was using FlowJo software and cardiac populations were determined with population gating from isotype controls.

qRT-PCR. To assess mRNA transcript levels in hiPSC-CM populations, total RNA was extracted using a RNeasy Mini Kit (QIAGEN). Superscript III First Strand Synthesis (ThermoFisher) was used to generate cDNA and qRT-PCR was performed on ViiA 7 Real-Time PCR Machine (Applied Biosystems) with SYBR Green PCR Master Mix (ThermoFisher). Transcript copy numbers were calculated using 2-ΔΔCt method with normalization to *HPRT1* housekeeping gene. Primers used in this study were *ASIC1* forward 5'-GGATGGAGGTCTACCCTGGA-3' and reverse 5'-GACCTCAGCTTCTGCCTGTCA-3' and *HPRT1* forward 5'-TGACACTGGCAAAACAATGCA-3' and reverse 5'GGTCCTTTTCACCAGCAAGCT-3'.

Immunohistochemisty/TUNEL stain. After overnight treatment at low pH, replated hiPSC-CMs were fixed in 4% paraformaldehyde for 10 min, washed in PBS, and incubated for 1 h at room temperature in blocking solution (PBS containing 2% heat-inactivated sheep serum (HISS) and 0.05% Triton X-100). Cells were incubated overnight at 4°C with primary antibody followed by incubation with secondary antibody for 1 h at room temperature. Nuclei were counterstained with 1 µg/mL DAPI. The samples were washed with PBS and TUNEL stain (Abcam) was performed as per manufacturer protocol. Stained samples were imaged within one week. All antibody dilutions were prepared in blocking solution. The following antibodies were used: mouse anti-α-actinin (Clone EA-53, Sigma Aldrich, 1:100) and donkey anti-mouse AlexaFluor 647 (ThermoFisher, 1:100). High-resolution images were obtained using a Zeiss LSM710 AiryScan confocal microscope with 20x 0.8 NA or 40x 1.3 NA Plan Apochromat objectives running Zeiss Zen Black. All image processing and quantitation was performed in FIJI (*85*).

Patch clamp analysis of cardiac ion channels. Off target analysis of Hi1a inhibition on cardiac ion channels was performed by Eurofins **(Supplemental Table 1)**. In each experiment the respective reference compounds were tested concurrently with the test compounds, and the data were compared with historical values determined at Eurofins. The experiment was accepted in accordance with Eurofins Standard Operating Procedure on assay validation. Electrophysiological assays conducted to profile Hi1a for activities on the ion channel targets hNav1.5, hKv4.3/hKChIP2, hCav1.2, hNav1.5, hERG, hKCNQ1, and hKir2.1 using the QPatch electrophysiological platform. Where presented, IC_{50} values were determined by a non-linear, least squares regression analysis. Reference standards were run as an integral part of each assay to ensure the validity of the results obtained. Results showing an inhibition (or stimulation) higher than 50% are considered to represent significant effects of Hi1a. **CYL8004QP2 Nav1.5 Human Sodium Ion Channel Cell Based QPatch CiPA Assay:** Onset and steady state block of peak Nav1.5 current is measured using a pulse pattern, repeated every 5 sec, consisting of a hyperpolarizing pulse to -120 mV for a 200ms duration, depolarization to -15mV amplitude for a 40ms duration, followed by step to 40mV for 200ms and finally a 100ms ramp (1.2 V/s) to a holding potential of -80mV. Peak current is measured during the step to -15mV. Leak current is measured at the step pulse from -120mV to -130mV. **CYL8069QP2Kv4.3 /KChIP2 Human Potassium Ion Channel Cell Based QPatch CiPA Assay:** The parameters measured were the maximum outward current (peak and end) evoked on stepping from -80mV to 40mV from the test pulse. This paradigm is delivered once every 5s to monitor the current amplitude. **CYL8051QP2Cav1.2 (L-type) Human Calcium Ion Channel Cell Based QPatch CiPAAssay:** After whole cell configuration is achieved, a 50ms step pulse from -60mv to 10mV in 15s intervals for a total of three pulses were applied and inward peak currents were measured upon depolarization of the cell membrane. Following the addition of compound five pulses of -80mV to -60mV for 5000ms was applied prior to the three step pulses. **CYL7004QP2 Nav1.5 Late Current Human Ion Channel Cell Based Antagonist QPatch CiPA Assay:** The parameters measured were the maximum inward current (Charge) evoked 5ms after stepping to -15mV from the test pulse and maximum inward current (Charge) during the ramp activated with 100nM ATXII. **CYL8038QP2 hERG Human Potassium Ion Channel Cell Based QPatch CiPA Assay**: After whole cell configuration is achieved, the cell is held at -80 mV. A 500 ms pulse to -40 mV is delivered to measure the leaking current, which is subtracted from the tail current on-line. Then the cell is depolarized to +40 mV for 500ms and then to -80 mV over a 100ms ramp to elicit the hERG tail current. This paradigm is delivered once every 8s to monitor the current amplitude. **CYL8007QP2KCNQ1/hminK Human Potassium Ion Channel Cell Based QPatch CiPA Assay**: After whole cell configuration is achieved, a 1000ms pulse from -80mv to 60mV then a ramp for 60mV to -80mV over 115ms was applied and outward peak currents were measured upon depolarization of the cell membrane. This paradigm is delivered once every 15s to monitor the current amplitude. **CYL8032QP2Kir2.1 Human Potassium Ion Channel Cell Based QPatch CiPA Assay:** The parameters measured were the maximum inward current (peak and end) evoked on stepping down from -30mV to - 120mV for 500ms. This paradigm is delivered once every 20s to monitor the current amplitude.

Computational analysis of human translatome data. Transcriptional (mRNA-seq) and translational (Ribo-seq) raw data of human heart were obtained from the Hubner Lab website (http://shiny.mdc-berlin.de/cardiac-translatome/) (*53*). Quality control checks for both RNA-seq and Ribo-seq data sets were performed to ensure reasonable quality for downstream analysis. Genes that were expressed in > 99% of samples were retained. After quality control, 47,094 and 43,183 genes were retained in the RNA-seq and Ribo-seq datasets, respectively. DESeq2 normalization was applied to normalize sequencing depth and RNA composition. The detailed normalization workflow performed by DESeq2 (*86*) involved four steps. First, calculated row-wise geometric mean (pseudo-reference sample) by square root of the product of all expression values across samples for each gene. Second, the ratio of each sample to the row-wise geometric mean was calculating by dividing the expression value of every gene by their row-wise geometric mean within a sample. Third, the normalization factor was calculated for each sample, which is the median value of all ratios for a sample. Lastly, the normalized count was calculated using the normalization factor, in which each raw count in a sample was divided by the normalization factor of that sample, and this was performed for every gene in every sample. The normalized counts were log-transformed to eliminate the effect of extreme values. A total of 80 samples were analysed, including a dilated cardiomyopathy group (65 samples) and control group (15 samples). We utilized R package ggplot2 (v3.2.1) (*87*) with box and violin plot to generate the two conditions in one graph for the genes encoding ASIC1, ASIC2, ASIC3, and ASIC4, in order to visualize the distribution of gene expression within one group and compare expression differences between groups.

SUPPLEMENTAL FIGURES

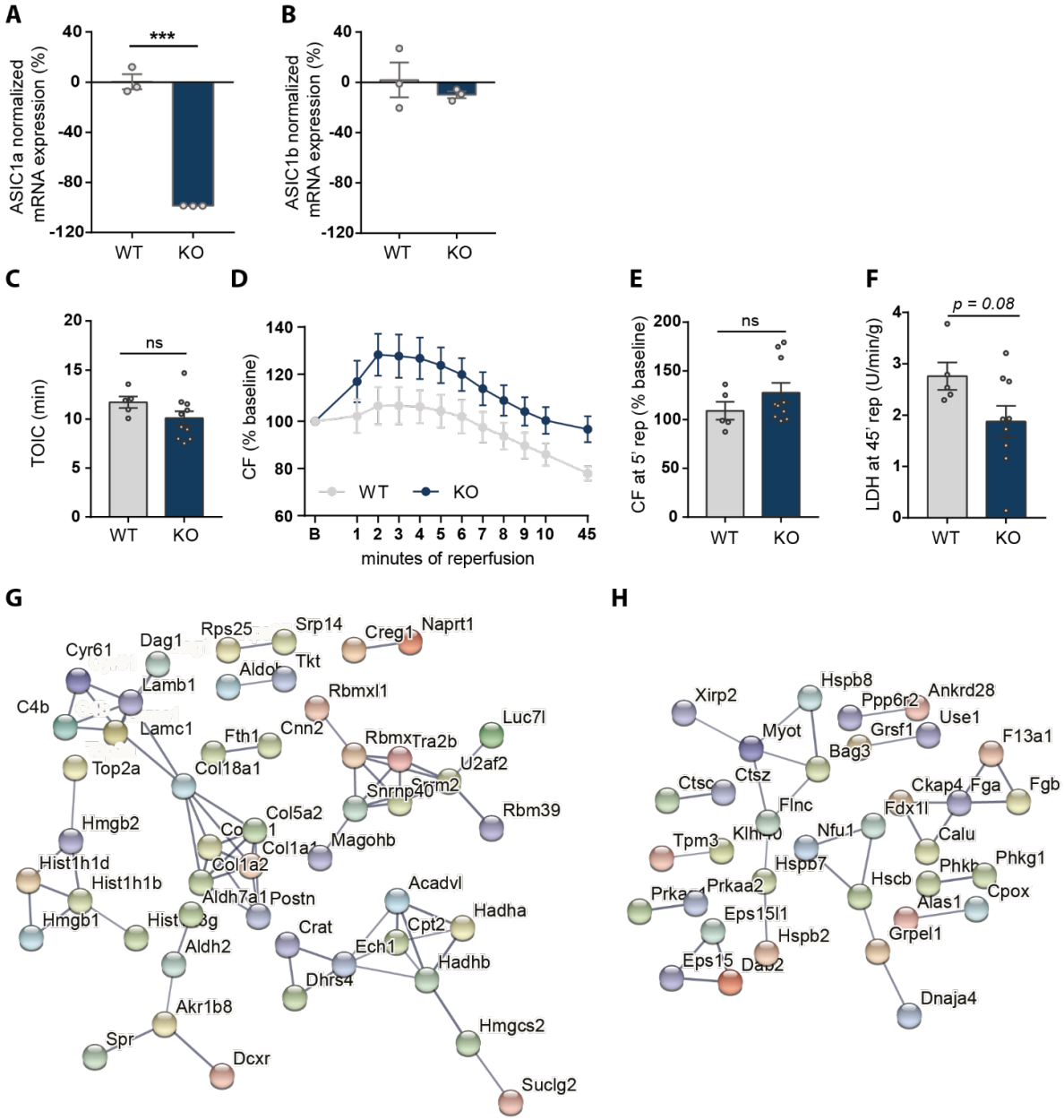

Supplemental Figure 1. ASIC1a knockout mouse analysis. **(A-B)** Normalized mRNA expression levels of **(A)** ASIC1a ($p<0.0001$, WT 0.3 ± 6.0%, ASIC1a$^{-/-}$ –98.7 ± 0.7%) and **(B)** ASIC1b ($p=45$, WT 1.9 ± 13.8%, ASIC1a$^{-/-}$ –9.9 ± 2.6%) from brain samples from WT (black, $n = 3$) and ASIC1a$^{-/-}$ mice (green, $n = 3$). Statistical significance was determined with two-tailed unpaired Student's *t*-test (***$p<0.001$). Data are presented as mean ± SEM. **(C-G)** Hearts from ASIC1a KO (ASIC1a$^{-/-}$, $n = 10$, dark gray) and WT (ASIC1a$^{+/+}$, $n = 5$, light grey) mice were subjected to 25 min of global ischemia followed by 45 min of reperfusion. **(C)** Time to onset of ischemic contracture (TOIC, $p = 0.162$). **(D)** Coronary flow (CF) at baseline (B, pre-ischemia), during the first 10 min of reperfusion, and at the end of the 45 min reperfusion period. **(E)** CF at 5 min reperfusion ($p = 0.26$). **(F)** Cell death after 45 min of reperfusion (units of LDH normalized to reperfusion flow rate and heart weight, U/min/g, $p = 0.08$). For all parameters, baseline values were obtained immediately prior to ischemia, and all data are expressed as mean ± SEM. Statistical significance was evaluated with two-tailed unpaired Student's *t*-test (*$p < 0.05$). **(G-H)** STRING analysis showing proteins significantly increased **(G)** and decreased **(H)** in ASIC1a KO hearts compared to WT hearts.

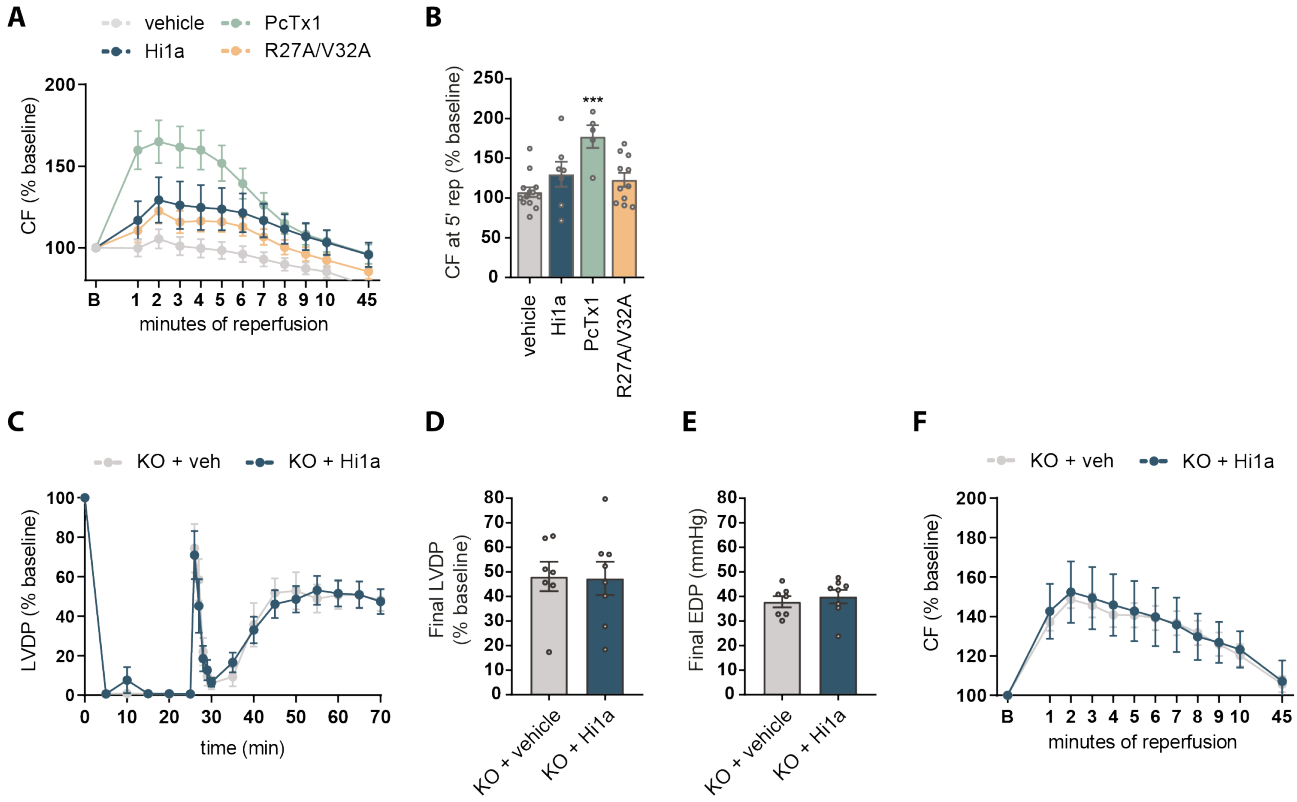

Supplemental Figure 2. ASIC1a inhibitors protect mouse hearts from *ex vivo* IRI. **(A-B)** Additional analysis of the experiment described in Figure 2. **(A)** CF plotted versus time (min) at baseline (B, pre-ischemia), during the first 10 min of reperfusion, and at the end reperfusion (45 min). **(B)** CF at 5 min reperfusion. Statistical significance was determined using one-way ANOVA with multiple comparisons (***p < 0.001). Data are presented as mean ± SEM (n > 5/group). **(C-F)** ASIC1a inhibitors do not significantly increase recovery of function in ASIC1a KO hearts (n = 7 – 8/group) based on measures of LVDP **(C-D)**, EDP **(E)**, and CF **(F)**.

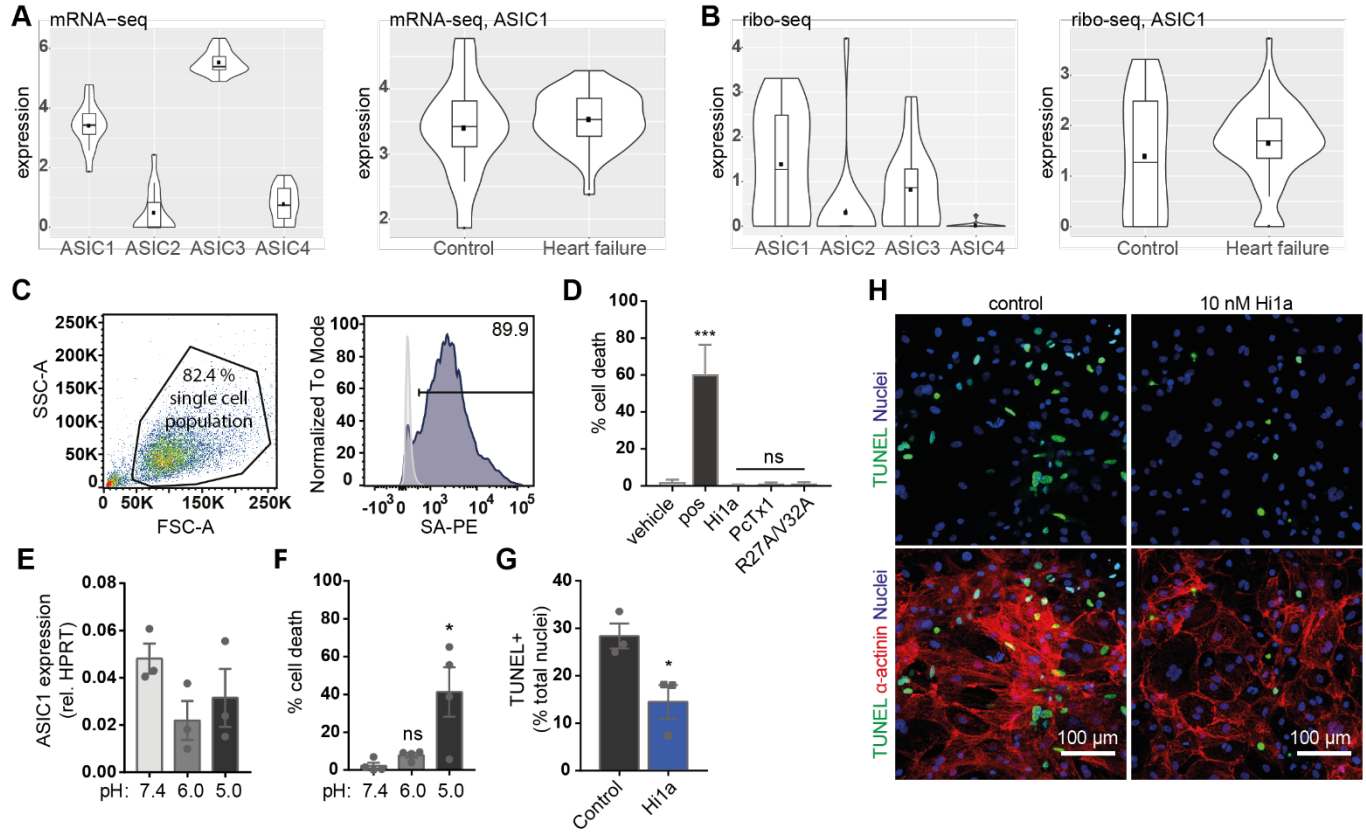

Supplemental Figure 3. ASIC expression in human heart muscle. Analysis of published **(A)** transcriptomic (mRNA-seq) and **(B)** translatomic (ribo-seq) data from the left ventricles of control (n = 15) and heart failure (dilated cardiomyopathy) (n = 65) patients (*53*). Data are presented as box blots where the middle box represents interquartile range (IQR), the middle line in the box is median (50th percentile of the data set), and points outside the plot are outliers. **(C-G)** Generation of hiPSC-CMs and treatment at low pH. **(C)** Flow cytometry analysis of differentiated hiPSC-CMs prior to replating. Single cell population from SSC-A (side scatter) versus FSC-A (forward scatter) plot (left) was analysed for the percentage of cells that stained positive for sarcomeric α-actinin (SA, PE-gated population) shown as a histogram (middle) and a scatter plot against an unstained fluorophore (right). Isotype-stained sample (grey) was used to create PE+ gate to analyse SA stained sample (blue). (**D**) Replated hiPSC-CMs treated for 48 hours in RPMI + B27 with vehicle (0.1% BSA in water), positive control (10 μM thapsigargin), 10 nM Hi1a, 10 nM PcTx1, or 10 nM PcTx1 R27A/V32A and evaluated for cell death (LDH) **(E-F)** Replated hiPSC-CMs treated overnight in HBSS at pH 7.4, 6.0, or 5.0 and analysed for **(E)** mRNA expression (qRT-PCR) of ASIC1 and **(F)** cell death (LDH). **(G-H)** Replated hiPSC-CMs treated overnight in HBSS at pH 5.0 with **(G)** quantification of cell death (TUNEL-positive nuclei normalized to total nuclei) following **(H)** immunohistochemistry for TUNEL (green) and α-actinin (red) with nuclei counterstained with DAPI. Top panel: TUNEL and DAPI merged image. Bottom panel: TUNEL, α-actinin, and DAPI merged image. All data are expressed as mean ± SEM (n = 3 biological replicates, 2–3 technical replicates each). Statistical significance was determined with one-way ANOVA (LDH results, panel c) or with a two-tailed unpaired student's t-test (TUNEL quantification, panel d) (*$p < 0.05$).

Supplemental Table 1. Eurofins data of patch clamp electrophysiology results for off target inhibition of cardiac ion channel currents

hNav1.5

Compound ID	Client Compound ID	Batch Number	Concentration (µM)	% inhibition			
				n1	n2	n3	mean
US034-0009110-1	Hi1a WT		1	7.31	10.96	7.10	8.46
Time-Matched Vehicle Control	DMSO		0.003	5.81	3.48		4.65
Time-Matched Vehicle Control	DMSO		0.003	5.88	8.34		7.11
Time-Matched Vehicle Control	DMSO		0.003	6.00	13.39		9.70
Time-Matched Vehicle Control	DMSO		0.003	6.94	16.38		11.66
Time-Matched Vehicle Control	DMSO		0.003	14.55	20.06		17.31
Positive Reference Control	Tetracaine		0.03	6.26	6.62		6.44
Positive Reference Control	Tetracaine		0.3	28.83	25.58		27.20
Positive Reference Control	Tetracaine		3	74.19	68.47		71.33
Positive Reference Control	Tetracaine		30	93.85	88.76		91.30
Positive Reference Control	Tetracaine		300	96.60	95.17		95.88

hKv4.3/hKChIP2

Compound ID	Client Compound ID	Measurement	Concentration (µM)	% inhibition			
				n1	n2	n3	mean
US034-0009110-1	Hi1a WT	Peak	1	7.01	10.29	2.15	6.48
Time-Matched Vehicle Control	DMSO	Peak	0.003	9.52	10.19		9.85
Time-Matched Vehicle Control	DMSO	Peak	0.003	9.44	10.74		10.09
Time-Matched Vehicle Control	DMSO	Peak	0.003	10.53	11.25		10.89
Time-Matched Vehicle Control	DMSO	Peak	0.003	11.69	13.62		12.66
Time-Matched Vehicle Control	DMSO	Peak	0.003	12.91	14.91		13.91
Positive Reference Control	Flecainide	Peak	0.03	7.41	10.98		9.20
Positive Reference Control	Flecainide	Peak	0.3	4.05	12.76		8.40
Positive Reference Control	Flecainide	Peak	3	10.63	14.48		12.55
Positive Reference Control	Flecainide	Peak	30	57.45	53.03		55.24
Positive Reference Control	Flecainide	Peak	300	97.40	97.33		97.37
US034-0009110-1	Hi1a WT	End	1	6.42	9.65	-2.27	4.60
Time-Matched Vehicle Control	DMSO	End	0.003	8.79	9.35		9.07
Time-Matched Vehicle Control	DMSO	End	0.003	7.83	11.49		9.66
Time-Matched Vehicle Control	DMSO	End	0.003	13.16	15.82		14.49
Time-Matched Vehicle Control	DMSO	End	0.003	8.79	18.01		13.40
Time-Matched Vehicle Control	DMSO	End	0.003	10.10	19.62		14.86
Positive Reference Control	Flecainide	End	0.03	5.29	8.57		6.93
Positive Reference Control	Flecainide	End	0.3	2.84	11.49		7.17
Positive Reference Control	Flecainide	End	3	25.60	27.93		26.76
Positive Reference Control	Flecainide	End	30	69.25	74.44		71.84
Positive Reference Control	Flecainide	End	300	90.01	90.99		90.50

hCav1.2

Compound ID	Client Compound ID	Batch Number	Concentration (µM)	% inhibition			
				n1	n2	n3	mean
US034-0009110-1	Hi1a WT		1	2.79	13.20	10.94	8.98
Time-Matched Vehicle Control	DMSO		0.003	4.58	6.34		5.46
Time-Matched Vehicle Control	DMSO		0.003	16.52	18.39		17.45
Time-Matched Vehicle Control	DMSO		0.003	18.02	21.14		19.58
Positive Reference Control	Nifedipine		0.001	21.65	8.54		15.09
Positive Reference Control	Nifedipine		0.01	38.19	31.48		34.83
Positive Reference Control	Nifedipine		0.1	53.13	58.25		55.69
Positive Reference Control	Nifedipine		1	56.76	65.20		60.98
Positive Reference Control	Nifedipine		10	81.42	86.13		83.78
Positive Reference Control	Nifedipine		100	95.15	94.45		94.80

hNav1.5 Late current antagonist assay

Compound ID	Client Compound ID	Batch Number	Concentration (µM)	% inhibition			
				n1	n2	n3	mean
US034-0009110-1	Hi1a WT		1	-9.74	-13.93	-13.45	-12.37
Time-Matched Vehicle Control	ATXII		0.1	12.22	12.95		12.59
Time-Matched Vehicle Control	ATXII		0.1	12.69	11.67		12.18
Time-Matched Vehicle Control	ATXII		0.1	12.21	-1.06		5.57
Positive Reference Control	Ranolazine		1	6.36	5.73		6.04
Positive Reference Control	Ranolazine		3	18.25	20.77		19.51
Positive Reference Control	Ranolazine		10	39.00	33.34		36.17
Positive Reference Control	Ranolazine		30	53.79	54.57		54.18
Positive Reference Control	Ranolazine		100	80.54	81.39		80.97
Positive Reference Control	Ranolazine		300	95.69	95.31		95.50

hERG

Compound ID	Client Compound ID	Batch Number	Concentration (μM)	% inhibition			
				n1	n2	n3	mean
US034-0009110-1	Hi1a WT		1	-7.50	1.58	-12.68	-6.20
Time-Matched Vehicle Control	DMSO		0.003	-8.30	0.64		-3.83
Time-Matched Vehicle Control	DMSO		0.003	-8.37	2.77		-2.80
Time-Matched Vehicle Control	DMSO		0.003	-6.85	5.17		-0.84
Time-Matched Vehicle Control	DMSO		0.003	-5.18	6.60		0.71
Time-Matched Vehicle Control	DMSO		0.003	-1.07	10.86		4.90
Positive Reference Control	E-4031		0.003	5.98	1.55		3.77
Positive Reference Control	E-4031		0.01	22.13	17.61		19.87
Positive Reference Control	E-4031		0.03	50.00	38.10		44.05
Positive Reference Control	E-4031		0.1	90.16	79.29		84.72
Positive Reference Control	E-4031		0.3	98.67	93.69		96.18

hKCNQ1/mink

Compound ID	Client Compound ID	Batch Number	Concentration (μM)	% inhibition			
				n1	n2	n3	mean
US034-0009110-1	Hi1a WT		1	1.87	-0.67	-0.68	0.17
Time-Matched Vehicle Control	DMSO		0.003	4.27	1.17		2.72
Time-Matched Vehicle Control	DMSO		0.003	-1.91	5.71		1.90
Time-Matched Vehicle Control	DMSO		0.003	-1.47	12.48		5.51
Positive Reference Control	Chromanol 293B		0.3	1.35	7.13		4.24
Positive Reference Control	Chromanol 293B		1	9.45	15.04		12.25
Positive Reference Control	Chromanol 293B		3	21.34	24.36		22.85
Positive Reference Control	Chromanol 293B		10	39.37	41.20		40.28
Positive Reference Control	Chromanol 293B		30	74.46	73.39		73.92
Positive Reference Control	Chromanol 293B		100	96.45	95.16		95.80

hKir2.1

Compound ID	Client Compound ID	Measurement	Concentration (μM)	% inhibition			
				n1	n2	n3	mean
US034-0009110-1	Hi1a WT	Peak	1	1.94	-0.02	-0.97	0.31
Time-Matched Vehicle Control	DMSO	Peak	0.003	-5.63	0.05	-	-2.79
Time-Matched Vehicle Control	DMSO	Peak	0.003	-4.98	1.50	-	-1.74
Time-Matched Vehicle Control	DMSO	Peak	0.003	-3.13	6.70	-	1.78
Positive Reference Control	Barium	Peak	0.3	1.78	2.96	-	2.37
Positive Reference Control	Barium	Peak	1	7.99	4.90	-	6.45
Positive Reference Control	Barium	Peak	3	14.88	10.25	-	12.57
Positive Reference Control	Barium	Peak	10	16.68	9.94	-	13.31
Positive Reference Control	Barium	Peak	30	38.78	25.19	-	31.99
Positive Reference Control	Barium	Peak	100	63.60	61.68	-	62.64
US034-0009110-1	Hi1a WT	End	1	1.81	-0.51	-3.14	-0.62
Time-Matched Vehicle Control	DMSO	End	0.003	-5.71	-0.06	-	-2.89
Time-Matched Vehicle Control	DMSO	End	0.003	-6.61	1.59	-	-2.51
Time-Matched Vehicle Control	DMSO	End	0.003	-6.64	8.78	-	1.07
Positive Reference Control	Barium	End	0.3	6.49	7.53	-	7.01
Positive Reference Control	Barium	End	1	19.93	16.65	-	18.29
Positive Reference Control	Barium	End	3	39.87	42.88	-	41.38
Positive Reference Control	Barium	End	10	79.79	81.66	-	80.72
Positive Reference Control	Barium	End	30	93.64	92.93	-	93.28
Positive Reference Control	Barium	End	100	98.46	98.47	-	98.46

Cardiac CiPA Reference Compound Panel

ITEM	Assay Name	Mode	Reference Compound	Estimated IC_{50} (μM)
CYL8004QP2DR	Nav1.5 Human Sodium Ion Channel Cell Based QPatch CiPA Assay	Antagonist	Tetracaine	0.94
CYL8038QP2DR	hERG Human Potassium Ion Channel Cell Based QPatch CiPA Assay	Antagonist	E-4031	0.032
CYL8007QP2DR	KCNQ1/minK Human Potassium Ion Channel Cell Based QPatch	Antagonist	Chromanol 293B	11.5
CYL8032QP2DR	Kir2.1 Human Potassium Ion Channel Cell Based QPatch CiPA Assay	Antagonist	Barium Chloride	62.3 (Peak) & 3.6 (End)
CYL8069QP2DR	Kv4.3 /KChIP2 Human Potassium Ion Channel Cell Based QPatch CiPA Assay	Antagonist	Flecainide	22.5 (Peak) & 10.0 (End)
CYL8051QP2DR	Cav1.2 (L-type) Human Calcium Ion Channel Cell Based QPatch CiPA Assay	Antagonist	Nifedipine	0.090

CYL7004QP2DR	Nav1.5 Late Current Human Ion Channel Cell Based Antagonist QPatch CiPA Assay	Antagonist	Ranolazine	20.1